Department of Complexity Science and Engineering
Graduate School of Frontier Sciences
The University of Tokyo

2022

Master's Thesis

Study on the orbital evolution of Long-period comets by numerical simulations

(数値シミュレーションによる長周期彗星の軌道進化に関する研究)

Submitted March 1, 2023

Adviser: Lecturer Kazuo Yoshioka

佐々木　優斗
Yuto Sasaki

Abstract

Long-period comets are defined as comets whose periods are longer than 200 years. Some of them come very close to the sun for the first time, and are called “Dynamically New Comets” (hereafter, DNCs). They are comets that approach closer than the “snow line” for the first time. They maintain the information of the Solar system formation age because they have been scarcely affected by solar weathering. Therefore, the investigation of DNCs is an important clue to revealing the process of the Solar system formation. Here, DNCs need to be picked out from Long-period comets. As a criterion of DNCs, A’Hearn’s criterion, the original semi-major axis (a_0) $\geq$ 20,000 au is commonly used. This criterion is based on observations. However, theoretical analyses showed that the perihelion distance of Long-period comets periodically gets close to the sun, so a criterion considering the comets’ motion since the Solar system formation age is currently required.

In this study, we examined the relationship between the value of the original semi-major axis and the minimum perihelion distance of Long-period comets by simulating the motion of 7,000 model comets since the Solar system formation age by numerical simulations. As a result, in the case of applying the current DNC criterion, $a_0 \geq 20{,}000$ au, more than 10% of comets have a history of snow line approach. On the other hand, in the case of $a_0 \geq 60{,}000$ au, more than 95% of comets have never approached the snow line. Therefore, we propose $a_0 \geq 60{,}000$ au as a DNC criterion.

Moreover, the inclination and the eccentricity distribution are analyzed for never-approached comets. Consequently, the inclination of comets that are likely to be Dynamically New concentrates on 90°. Additionally, their eccentricity concentrates on around 1.0. The results support the results of previous research.

The appearance frequency of DNCs is important in comet studies and missions. In the case of applying $a_0 \geq 60{,}000$ au as the DNC criterion, more than 70% of the number of comets survive compared with in the case of applying $a_0 \geq 20{,}000$ au as the criterion. Therefore, this proposed criterion is realistic enough to apply to both the study of the science of the Solar system formation and the comet exploration missions.

和文要旨

長周期彗星は周期が 200 年以上のものと定義されている。これらの彗星の中には、太陽系形成時以降初めて太陽から約 2.7 au 地点にある「スノーライン」より内側に接近するものがあり、それらは “Dynamically New Comets”（以下、DNCs）と呼ばれる。DNCs は宇宙風化の影響をほとんど受けていないと考えられるため、太陽系形成時の情報を保っているとされる。ゆえに、DNCs を詳細に探査することで太陽系の形成過程や形成時の環境の理解につながる手がかりが得られる。ここで、DNCs の探査を行うにあたり、数多くの長周期彗星の中から対象天体として DNCs を正しく選別する必要がある。現在、DNCs の判別基準として、A’Hearn により提唱された、original semi-major axis (a_0) $\geq$ 20,000 au が広く用いられている。この基準は既知の彗星観測データをもとに構築されたものである。しかし、近年、解析解によるシミュレーションによって彗星の近日点距離は、長い軌道進化の過程で周期的に変動していることが示された。すなわち、彗星の過去のスノーライン以内への接近履歴は直近の軌道要素の値だけでなく、太陽系形成以降の全時間にわたる彗星の運動を考慮しなければならない。そこで、彗星の過去の運動まで考慮に入れた DNCs の基準の構築が要請されている。

本研究では、数値シミュレーションを用いて 7,000 個のモデル彗星の太陽系形成以降の運動を再現することで、長周期彗星の original semi-major axis の値と最小近日点距離の関係を調べ、DNCs である可能性を評価した。その結果、現在の DNCs の基準である、$a_0 \geq 20{,}000$ au の場合は 10%以上の数の彗星で過去に接近履歴がある、すなわち DNCs とは呼べないことが明らかになった。一方、$a_0 \geq 60{,}000$ au とした場合は 95%以上の彗星で接近履歴が無かった。この結果から、$a_0 \geq 60{,}000$ au を DNCs の基準として提唱する。

また、スノーライン以内への接近履歴が無い彗星について、それらの軌道傾斜角と離心率の分布を調べた。その結果、Dynamically New の条件を満たす彗星は軌道傾斜角 90 度付近で最も多くなることが分かった。同様に離心率については、1.0 付近で最多となった。これらの結果は解析解を用いた先行研究の結果を支持するものとなった。

DNCs の基準は将来の彗星研究や探査で用いられることが想定されるため、その基準による DNCs の発見数が一定数存在することも実用上重要である。本研究により新たに提唱した $a_0 \geq 60{,}000$ au という基準による DNCs 発見数は、現在の基準（$a_0 \geq 20{,}000$ au）をもとにした場合の 70%程度であった。このことから、提唱した基準は十分実用的なものであると言える。

Contents

1. Introduction

1.1. Formation of the Solar system and comets

1.1.1. The origin of comets

Plenty of solid particles are considered to have existed around the primordial sun approximately 4.6 billion years (4.6 Gyrs) ago. The particles gradually accumulated due to mutual attractive force, and they formed planetesimals of several dozens of kilometers. Most planetesimals had floated for a long time, but some of them accumulated repeatedly, and grew to be planets. The fate of the remaining planetesimals was different depending on their position. The planetesimals that existed around giant planets such as Jupiter were transported to a very far region by the effect of the gravity of the planet, and they were thrown into elliptic orbits whose semi-major axes are more than 10,000 au[1]. These planetesimals are considered to form the Oort cloud (Oort, 1950). On the other hand, planetesimals existed farther than Neptune (Approximately 30 au) scarcely collapsed each other, and were rarely affected by the gravity of giant planets, so they formed a disk-like dense region of small objects. This region is called the Edgeworth-Kuiper belt, and is considered to spread about from 30 au to 50 au from the sun. When small objects approach the observable area, the ones from the Oort cloud are observed as Long-period comets, and the ones from the Edgeworth-Kuiper belt are observed as Short-period comets (Vokrouhlický et al., 2019).

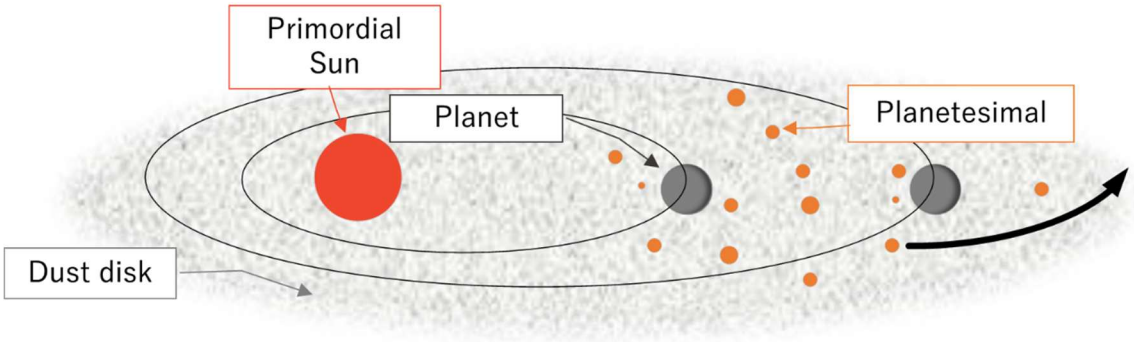

Fig. 1 Image of the initial era of the Solar system.
The planetesimals around the giant planets are transported to farther area.

[1] 1 au is approximately 1.5×10^8 km (150 million km).
Its origin is the average distance between the sun and the earth.

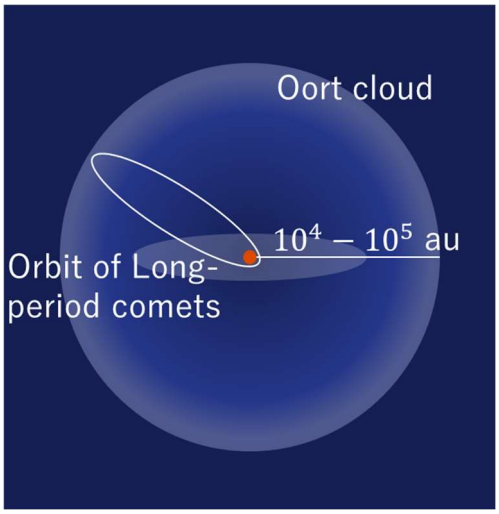

Fig. 2 Image of the Edgeworth-Kuiper belt and the Oort cloud.

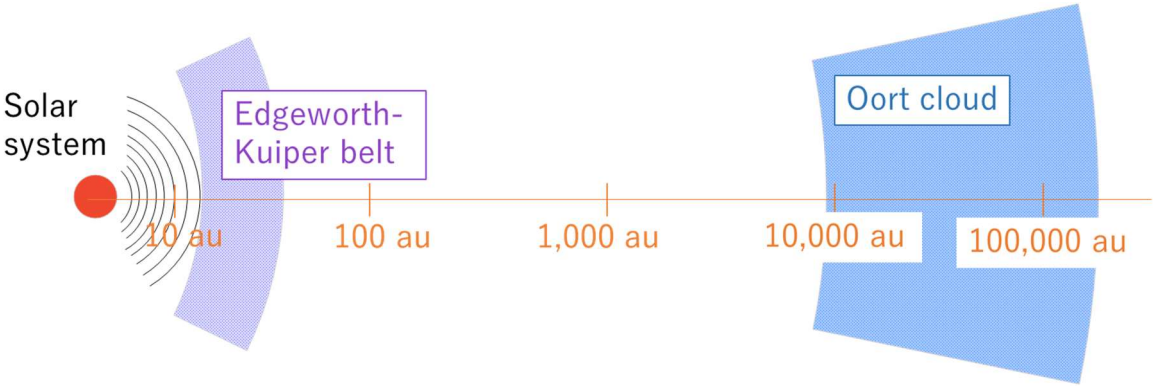

Fig. 3 Distance of the Edgeworth-Kuiper belt and the Oort cloud from the sun.
The Edgeworth-Kuiper belt spreads around 30-50 au from the sun.
The Oort cloud spreads farther than 10,000 au.

1.1.2. Long-period comets and the formation of the Oort cloud

The Oort cloud is considered to spread spherically around the area $10^4 - 10^5$ au from the sun. It is a dense region of small bodies, and is called "a reservoir of Long-period comets." The Oort cloud is estimated to contain about 10^{12} comets (Weissman, 1990). It is considered to be formed by the comets distributed spherically because of the effect of external forces. The formation process is shown below (Heisler & Tremaine, 1986).

【Formation process of the Oort cloud】

1. During the initial process of the Solar system formation, both planetesimals and planets exist.

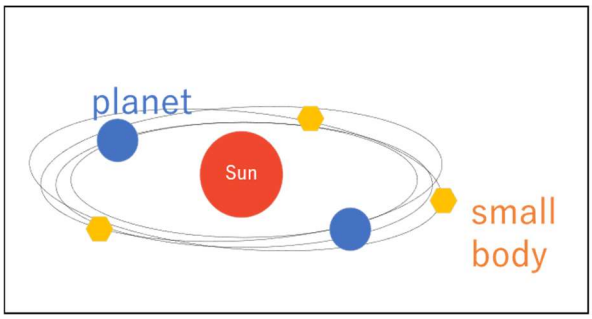

2. If a planetesimal pass near a planet, the planetesimal is accelerated by the gravity of the planet.

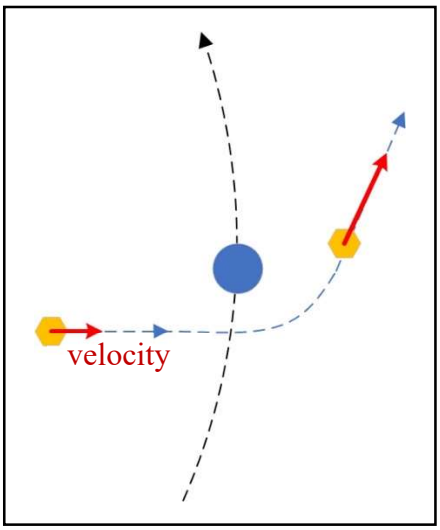

3. As the velocity gets large, the semi-major axis gets longer.
   It means the eccentricity gets larger.

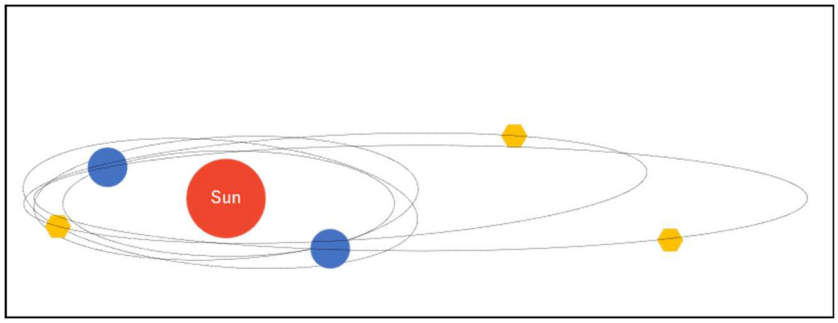

4. The farther the planetesimals were transported, the larger the effect of the Galactic tide will be. It leads to an increase in the inclination.

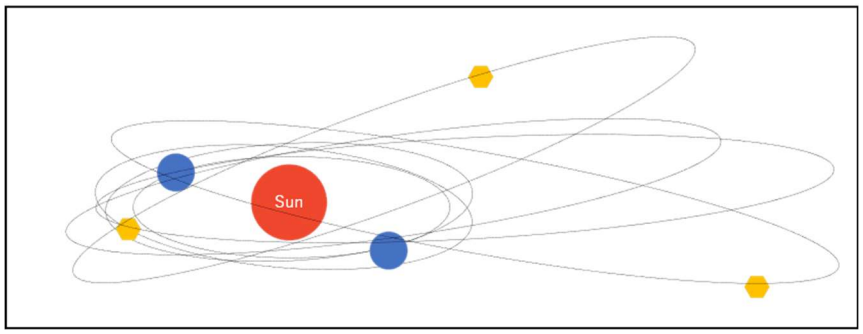

1.2. Classification of comets

1.2.1. Orbital elements

Orbital elements are parameters that are used to determine the orbit and position of celestial bodies. The parameters are as follows.

[The parameters that determine the shape of the orbit]

- Semi-major axis: a
- Eccentricity: e
  - $e = 0$: circle
  - $0 < e < 1$: ellipse
  - $e = 1$: parabola
  - $1 < e$: hyperbola

[The parameters that determine the plane of the orbit]

- Inclination: I
  - The angle between the reference plane and the orbital plane. In the case of comets, the ecliptic plane is often chosen as the reference plane.
- Longitude of the ascending node: Ω
  - The angle between the vernal equinox and the ascending node.

[The parameter that determines the direction of the orbit]

- Argument of perihelion: ω
  - The angle between the ascending node and the perihelion.

[The parameter that determines the position of the body]

- Time of perihelion passage: t_0
  - It is a parameter to determine the current position of the body in the orbit.

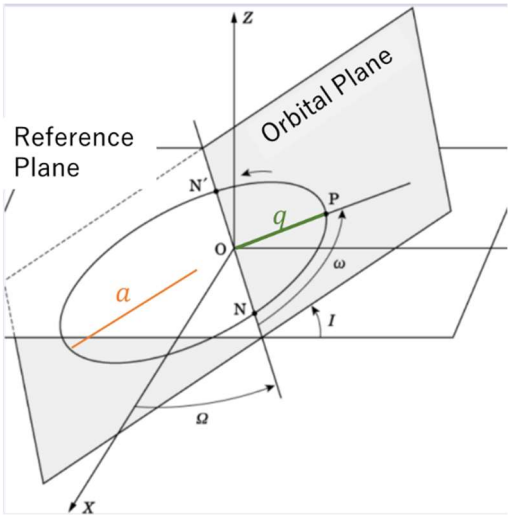

Fig. 4 Image of orbital elements.
(Original Source: Astronomical Society of Japan)

Here, as for the semi-major axis, three different symbols (a_i, a_0, a) are used properly depending on the semi-major axis at what time in this paper. The orbit of comets varies depending on the time because of perturbation effects from the planets. Therefore, the semi-major axis also fluctuates every moment.

First, a_i means the "Initial semi-major axis". It is the semi-major axis at the initial era of the Solar system, that is, about 4.5 billion years ago (Fig. 5 A). This also means the semi-major axis at the start point of calculation.

Second, a_0 means the "Original semi-major axis". It is the semi-major axis just before the previous approach to the planet region (Approximately 40 au) (Fig. 5 C). This value shows the current semi-major axis "without" perturbation.

Finally, a means the "(Current) semi-major axis". It is the semi-major axis at the observed time (Fig. 5 D).

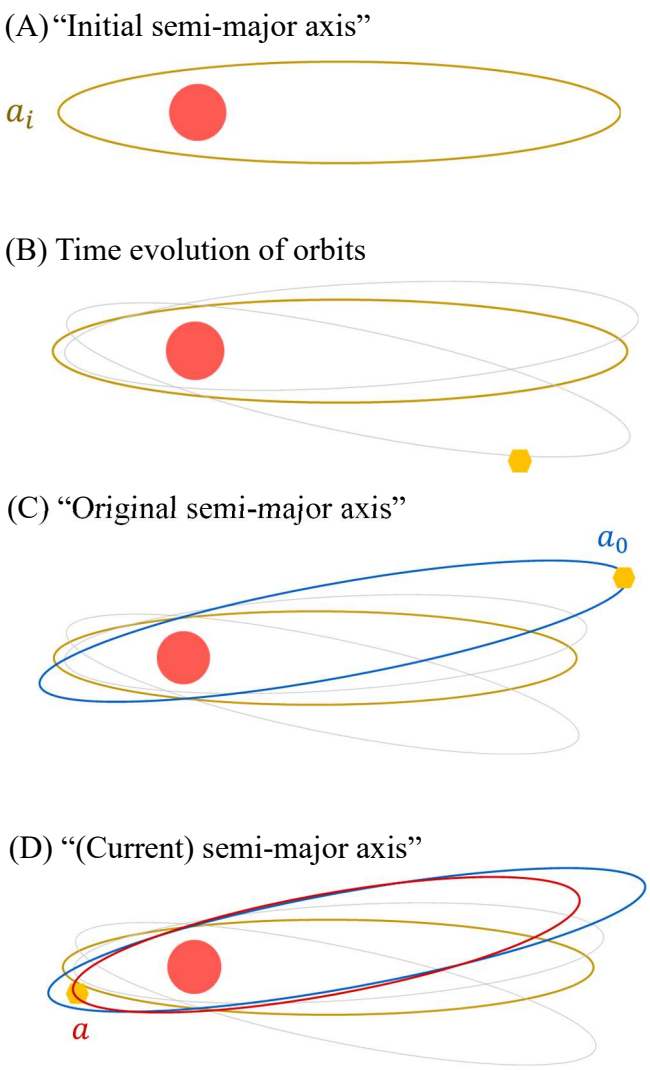

Fig. 5 Image of a_i , a_0 and a.

1.2.2. Classification of comets according to the orbital elements

Comets are classified mechanically based on the orbital elements. A commonly used classification by A'Hearn et al. (1995) is presented below.

Firstly, focusing on eccentricity, comets with $e < 1$ are called "Periodic comets". On the other hand, other comets are called "Non-periodic comets".

Periodic comets are classified further based on their periods – strictly speaking, the period is not an orbital element, but it is derived from the semi-major axis, which is one of the orbital elements –. Comets with $P \geq 200$ years are "Long-period comets", and those with $P < 200$ years are "Short-period comets".

Finally, Long-period comets are divided into three categories based on the original semi-major axis. Comets with $20{,}000\ \mathrm{au} \leq a_0$ are "Dynamically New comets", those with $500\ \mathrm{au} \leq a_0 < 20{,}0000\ \mathrm{au}$ are "Young, Long-period comets" and $a_0 < 500\ \mathrm{au}$ are "Old, Long-period comets".

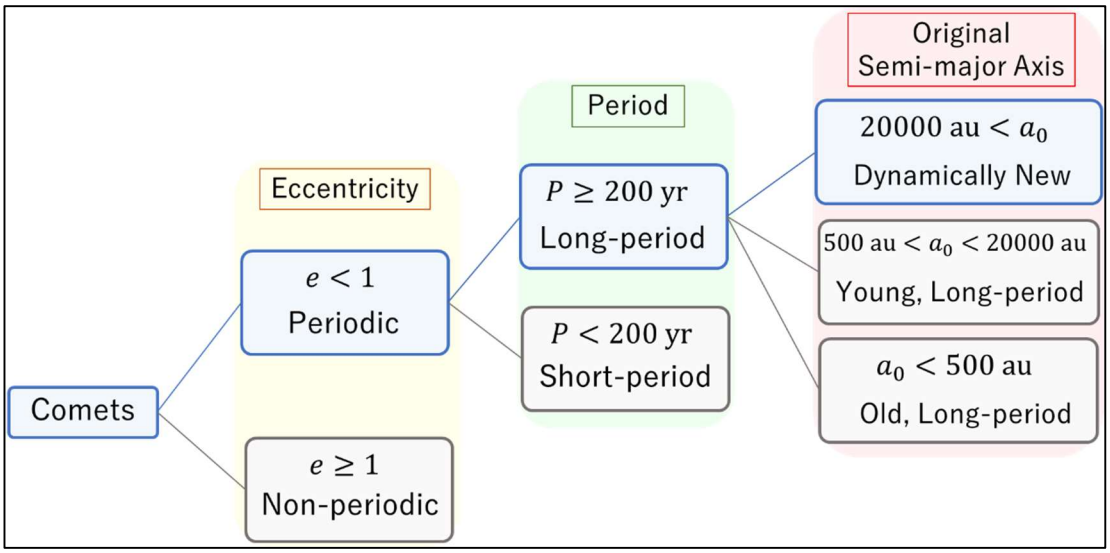

Fig. 6 Dynamical classes of comets. (Created based on A'Hearn et al., 1995)

1.2.3. The importance of Dynamically New Comets

Although the substances distribute on the surface of comets that exist near the sun sublimate easily because of the heat, those distribute on the surface of comets that exist in the far area remain in solid states. The border is called the “snow line”. The snow line is defined for each substance because the sublimation temperature differs depending on the substances. The snow line of H_2O in the Solar system is about 2.7 au from the sun.

Dynamically New Comets (hereafter, DNCs) are comets that approach closer than the snow line for the first time after the formation of the Solar system. It means that DNCs maintain the substances originating in the Solar system formation era without melting. Therefore, DNCs are regarded as important clues to reveal the process and the environment of the Solar system formation era.

1.3. Recent studies on comets

1.3.1. Discovery methods of comets and the ways of orbit determination

In the ancient age, people discovered comets with their naked eyes. In the 1600s, telescopes began to be used for discovery. After that, some famous scientists such as Newton (1687) and Halley (1705) tried to reveal the orbit of comets. In 1860s, Donati (1864) and Huggins (1868) made the first spectroscopic observations of comets, and they opened up the new study method of the constituents of comets (Festou et al., 2004).

In 1995, comet study faced a turning point. Some all-sky automated survey projects started in that year. The projects are divided into two categories depending on the means. One is by telescopes which are based on the ground, and the other is by probes.

The number of discovered comets increased thanks to these projects. For instance, SOHO, a solar observatory, enabled us to discover Kreutz Sungrazers, a group of comets that approach very close to the sun. As a result of that, the number of discovered comets has increased, and it reaches about 200 comets annually these years.

Fig. 7 shows the number of discovered Long-period comets by decade (Jet Propulsion Laboratory[2]).

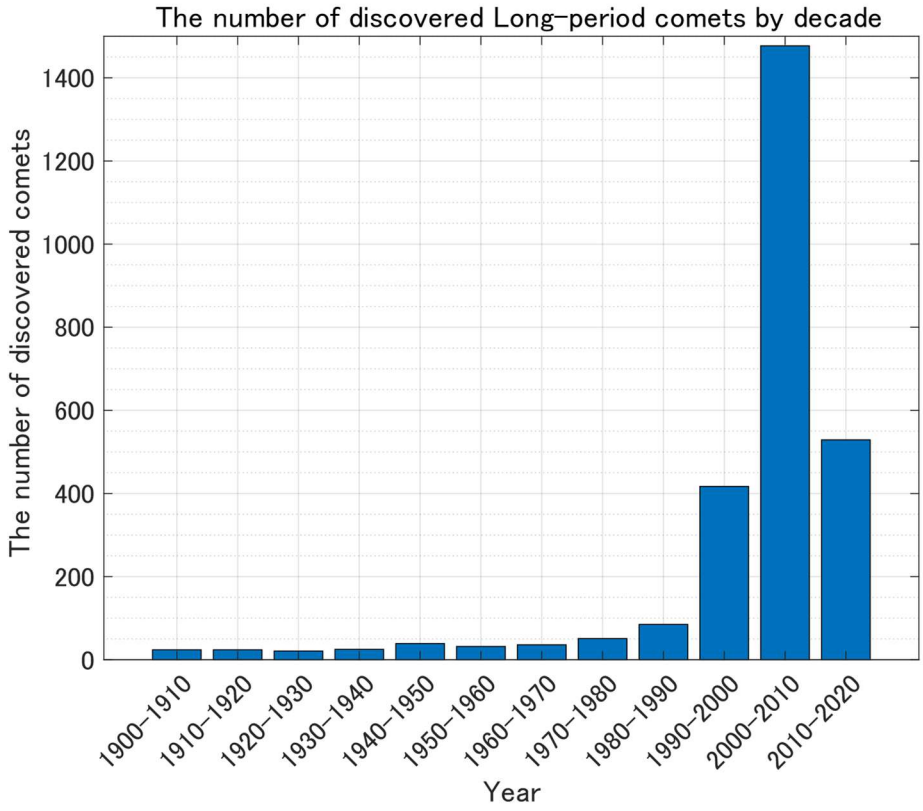

Fig. 7 The number of discovered Long-period comets by decade. (Created based on JPL)

[2] Jet Propulsion Laboratory (JPL), NASA.
https://www.jpl.nasa.gov/

Some examples of the leading all sky automated survey projects are listed below.

Table 1 Examples of the leading all sky automated survey projects.

Project name	Start of operation	Category
NEAT	1995	Ground-based optical telescope
SOHO	1995	Solar observatory
LINEAR	1996	Ground-based optical telescope
Pan-STARRS	2008	Ground-based optical telescope

The orbit of comets is calculated by estimating a curve based on the arc data for a certain period of time. This orbit is called an “osculating orbit”, which is an orbit that the comet draws at the very time. In other words, the comet does not always draw the same orbit because Long-period comets are affected by external forces while they are flying (Eugene & Wiliam, 2008). Therefore, it is required to consider the effects of external forces to simulate the long-term trajectory of comets.

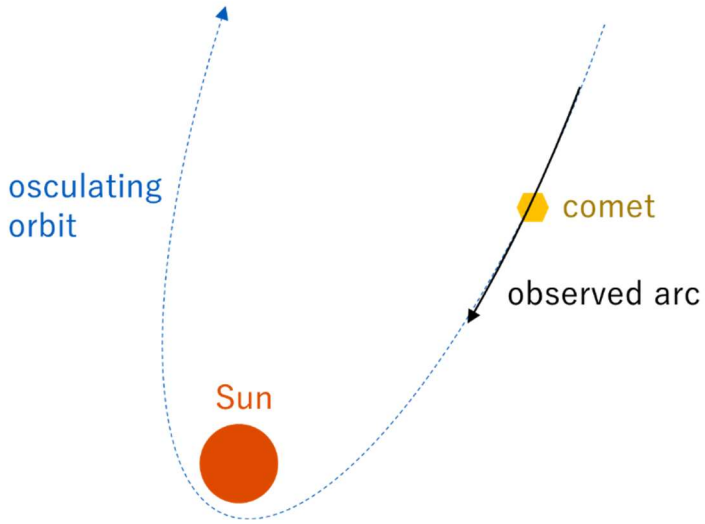

Fig. 8 Image of the orbit estimation.
The black line is the observed arc of the comet.
Based on the information of the arc, estimate the most suitable curve for the arc, which is the osculating orbit (the blue dotted line).

1.3.2. Candidates of “first-approaching” comets

The candidate of DNCs is not only Long-period comets but also interstellar objects. Since 2017, some interstellar objects such as ‘Oumuamua (1I/ 2017 U1) and Borisov (2I/ 2019 Q4) have been discovered. These objects existed very far area from the sun, so they are very important clues to reveal the process and environment of the Solar system formation era. However, these interstellar objects are rarely discovered. Therefore, focusing on only these objects is not sufficient and realistic to study the Solar system formation.

Here, another candidate of the “first-approaching” comets are DNCs categorized in Long-period comets. Recently, the number of discoveries of Long-period comets is increasing (Fig. 9). Therefore, investigating the scientific composition of DNCs is a realistic and promising method to understand the Solar system formation process.

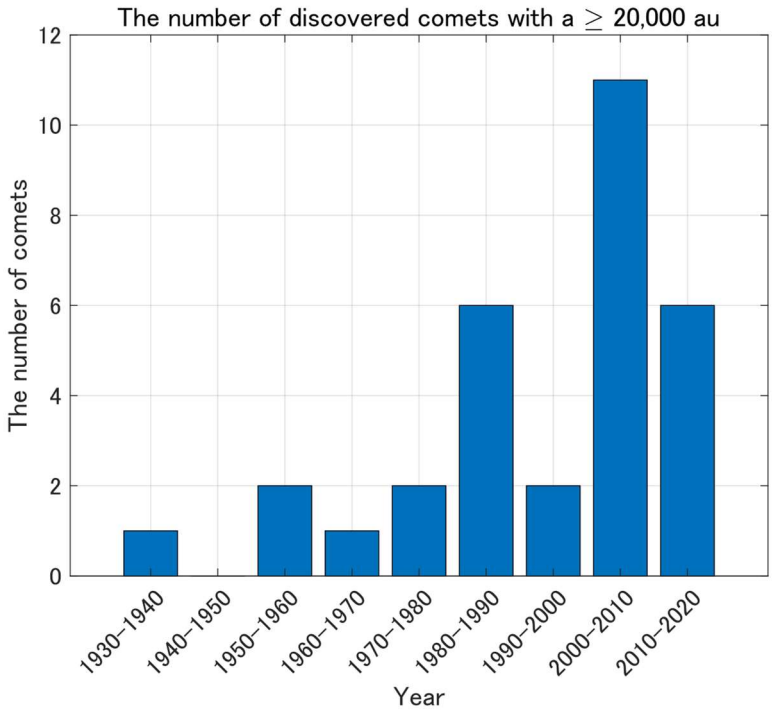

Fig. 9 The number of discovered comets with $\boldsymbol{a \geq 20,000}$ au by decade. (Source: JPL)
Each bin has the number of comets discovered in 10 years.
Here, we use the value of a, instead of that of a_0, since it is not realistic to calculate the value of a_0 for all discovered comets.

1.3.3. Previous studies on the dynamics of comets

A study on the motion of Long-period comets was essential to reveal the origin of the Oort cloud. There are two main methods for the study of the orbit of comets; one is based on the time evolution solutions and the other is based on the analytical solution. Each method has both strengths and weaknesses, so these two are used for different purposes.

The time evolution solution method is used to understand the dynamics of each comet. Oort (1950) showed the transportation process of planetesimals that existed near the giant planets to far regions due to the effect of the gravity of the planets in the early stage of the Solar system formation. Some years later, Heisler & Tremaine (1986) revealed the fact that the tidal force from the Galactic plane (Galactic tidal force) and the passing stars increase the inclination of transported planetesimals by the numerical simulation. Moreover, Duncan et al. (1987) simulated the Oort cloud formation process for the first time considering the effects of currently acknowledged external forces such as perturbations by planets, Galactic tidal force, and stellar encounters (Fig. 10). They tried to grasp the shape of the Oort cloud by the motion of planetesimals, which was obtained by solving the time evolution solution of the equation of motion for plenty of planetesimals for 4.5 billion years. As a result of that, they indicated that the Oort cloud can be divided into two regions in accordance with the distance; the region within 30,000 au from the sun is called the “inner Oort cloud”, and outer than 30,000 au is called the “outer Oort cloud”.
They found out that the inner Oort cloud has four to five times more comets than the outer Oort cloud.

These days, some scientists try to understand the macro-scale motion of plenty of comets. The motion of a large number of comets is calculated by analytical solution.
Kinoshita & Nakai (2007) succeeded to derive the general solution of orbital evolution of bodies including the effect of the perturbation by planets estimated by Kozai (1962). Shortly after that, Higuchi et al. (2007) succeeded to express the analytical solution more simply using special functions. Moreover, Higuchi & Kokubo (2015) improved the solution and revealed the characteristics of each orbital element of Long-period comets by considering the effect of stellar encounters. In addition, Higuchi (2020) showed that the aphelion direction of observable comets concentrates on two planes; the ecliptic plane and the empty ecliptic plane, which is the plane of z-axis symmetry. This means that the distribution of observable comets is not spherical. Besides, it discussed the time evolution of each orbital element by simulating the motion of 10,000 model comets for 4.5 billion years. The analysis of the time evolution of the perihelion distance showed that the perihelion distance fluctuates periodically. It means that even comets that do not approach closer than the snow line in recent years may have a history of approach in the ancient age (Fig. 11). Therefore, it indicates that it is insufficient to consider only the recent perihelion distance in case of discussing the history of snow line approach of comets, so it is required to consider the whole motion of comets after their birth.

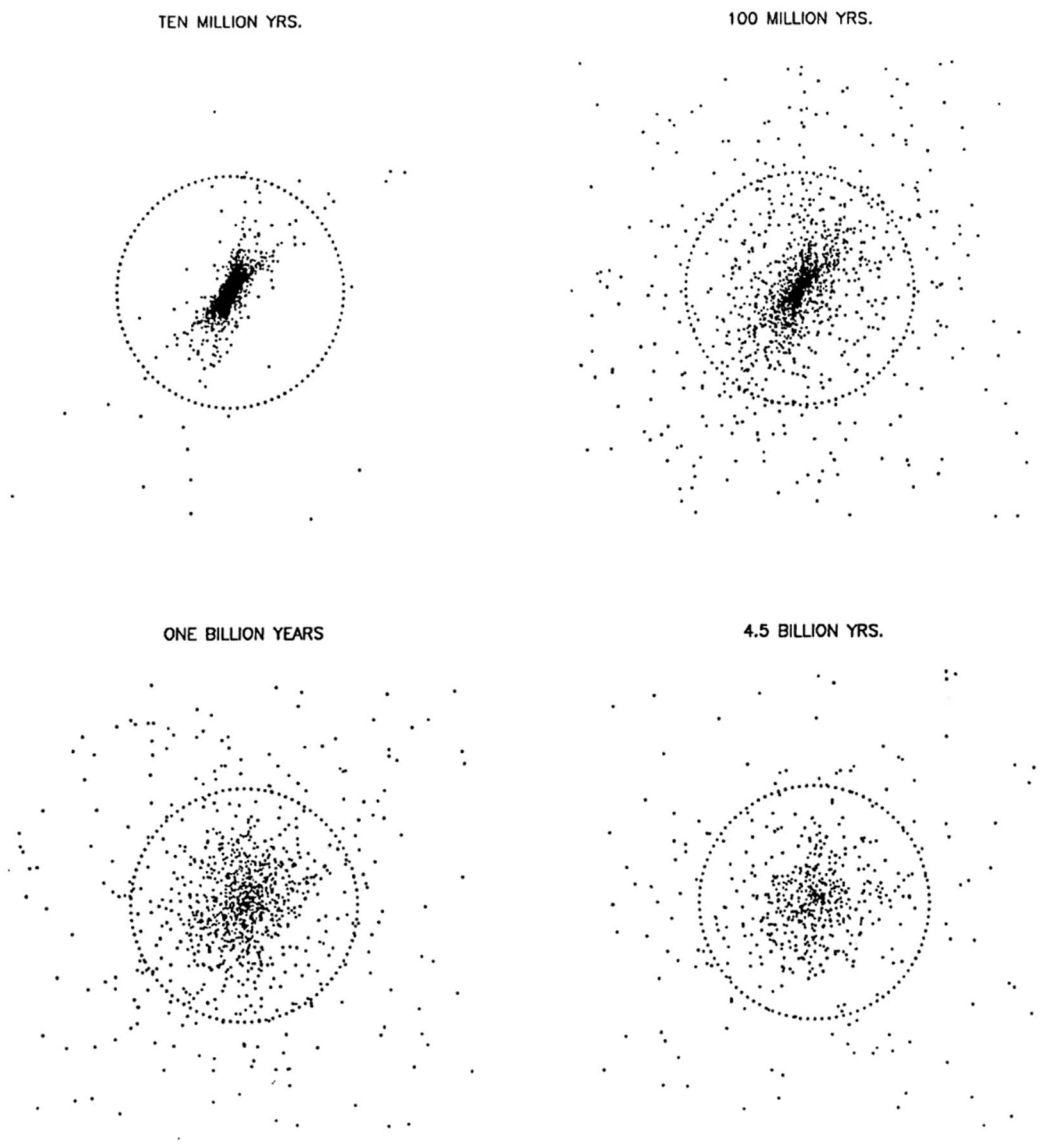

Fig. 10 The distribution of comets on several different times.
The horizontal direction is the Galactic plane. The dotted circle shows a radius of 20,000 au (Duncan et al., 1987).

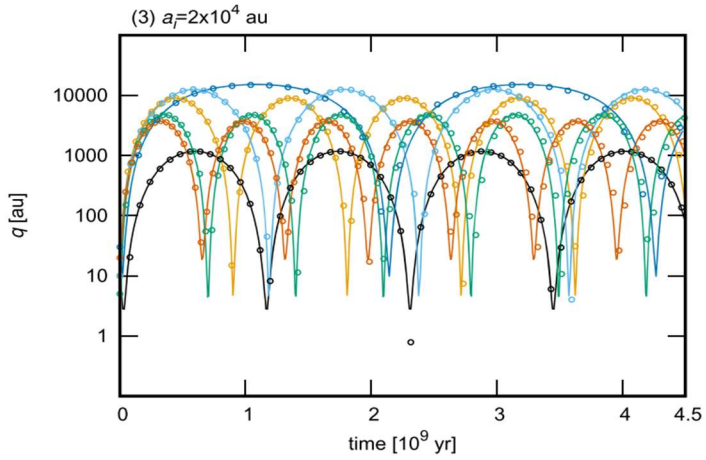

Fig. 11 The time evolution of the perihelion distance of comets with $a_i = 20,000$ au (Higuchi, 2020).
Each colored line has the different initial perihelion distance and the argument of perihelion. Regardless of the initial conditions, the perihelion distance fluctuates periodically.

There is a study that reevaluates the current criterion of DNCs, which is $a_0 \geq 20{,}000$ au. Królikowska & Dybczynski (2017) calculated the previous perihelion distance by tracing back the motion of comets which are 77 observed Long-period comets to the previous perihelion passage by numerical simulation. As a result, they concluded that comets which were not DNCs were included when the criterion was $a_0 \geq 20{,}000$ au. On the other hand, if the criterion was $a_0 \geq 40{,}000$ au, only DNCs included (Fig. 12). This study played an important role to make the DNC criterion more reliable, however, it left room for improvement in the points that the number of sample comets was very few and the motion of comets was traced back only to the previous perihelion passage time.

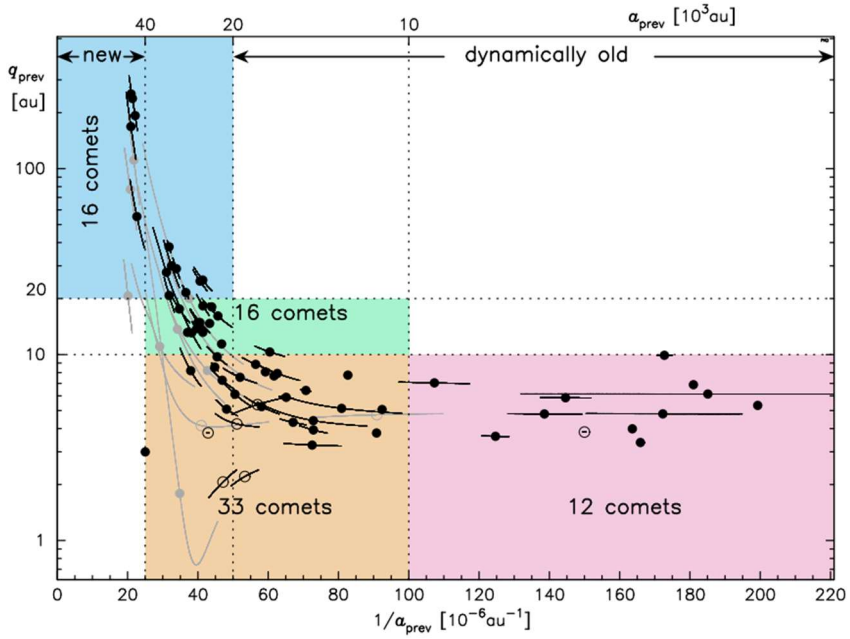

Fig. 12 Relationship between the previous perihelion distance and the previous semi-major axis (Królikowska & Dybczynski, 2017).
The scale above the graph shows the semi-major axis at the time of the previous perihelion passage ($\boldsymbol{a_{prev}}$). The scale on the left side of the graph shows the perihelion distance at the point of the previous approach ($\boldsymbol{q_{prev}}$).
The snow line in this paper is 20 au, considering substances that easily sublimate such as CO_2 and CO.
At $\boldsymbol{a_{prev} = 20{,}000}$ au, the perihelion distance of most comets is $\boldsymbol{q_{prev} < 20}$ au, which means NOT DNCs.
On the other hand, at $\boldsymbol{a_{prev} = 40{,}000}$ au all comets have $\boldsymbol{q_{prev} \geq 20}$ au, which means DNCs.

1.4. The objectives of this study and their importance

The objectives of this study are to reevaluate the current DNC criterion, which is $a_0 \geq 20{,}000$ au, and to estimate new parameters that reinforce the criterion.

In order to achieve this, in this study, the motion of comets was simulated for 5 billion years (5 Gyrs) by numerical simulations. Moreover, the characteristics of "first-approaching comets" were investigated. Here, the simulation method based on the time evolution solution is adopted for the calculation of comets' trajectory, considering the aim of the simulation, which is to simulate the motion of comets since the time of their birth.

This study contributes to both science and missions. As for science, it contributes to an accurate understanding of the environment at the age of Solar system formation. The scientific information on the Solar system formation era based on comets is obtained mainly from comets that have not been affected by space weathering. The target comets are often determined considering the current DNC criterion, but the criterion includes some not DNCs according to previous studies such as Królikowska & Dybczynski (2017). Here, if the information is obtained by comets that are not DNCs, the comets might have been affected by solar weathering so much. It may lead to misunderstanding of the Solar system formation process. Therefore, this study is expected to contribute to the correct understanding of that by making the DNC criterion more reliable.

In addition, this study may bring a great impact on the geological studies of the Solar system bodies. It is necessary to understand the denaturation process of the materials by solar weathering to predict the original state of the substances from their current states. There, the materials of the small bodies in the main belt are considered as important clues that provide us the information on the substances in the Solar system formation era (Bottke et al., 2005). However, the main belt lies from approximately 3 to 5 au from the sun, so the effects of solar weathering cannot be avoided completely. In order to solve that problem, the materials of DNCs can be used because they are rarely affected by solar weathering. Therefore, it contributes to the detailed understanding of the evolution process of substances in the Solar system.

In comet missions, as mentioned above, target comets must be the ones that have been rarely affected by solar weathering if the purpose of the mission is to reveal the formation process of the Solar system. In that point, this study contributes by bringing important implications to select DNCs.

2. Modeling of comets

2.1. The Fundamental theory of motion of comets

The forces applied to Long-period comets are gravity from the sun, Jupiter and nearby stars, and the Galactic tide.
The equation of motion is expressed as follows.

$$\frac{d^2\vec{r}}{dt^2} = -GM\frac{\vec{r}}{|\vec{r}|^3} - GM_J\frac{\overrightarrow{r_J}}{|\overrightarrow{r_J}|^3} + \sum_{s=1}^{N}\frac{GM_S(\overrightarrow{r_S}-\vec{r})}{|\overrightarrow{r_S}-\vec{r}|^3} - \nu_0^2\vec{z} \qquad (2-1)$$

From the first term to the third term on the right side are the gravitational force from the sun, Jupiter and nearby stars, respectively. The last term is the Galactic tidal force. Here, $\vec{r}$, $\vec{r}_J$ and $\vec{r}_S$ mean the position vector of the comet from the sun, Jupiter and the nearby stars, respectively. Moreover, M, M_J and M_S show the mass of them. Besides, as for the Galactic tidal force, we set $\nu_0 = \sqrt{4\pi G\rho}$, $\rho = 0.10M/\mathrm{pc}^3$ according to Binney & Tremaine (2008). See Section 2.2 for a detailed explanation of the Galactic tide. The information on nearby stars is based on the database Stellar Potential Perturbers Database (StePPeD)[3], which is a database on the stars that possibly perturb the bodies in the Solar system. It includes 788 possible stars.

In the case of Short-period comets, the non-gravitational force is also included as an external force. It is a force caused by sublimated gas. However, in the case of Long-period comets, this force can be neglected because Long-period comets do not get close to the sun so much. In Section 2.3.1, the effect of the non-gravitational force is evaluated in the case of Long-period comets, and it concluded that this effect can be neglected.

[3] https://pad2.astro.amu.edu.pl/StePPeD/index.php?n=Stars30.Downloads1

2.2. Galactic tidal force

The Milkey Way Galaxy (hereafter, the Galaxy) is composed of myriad celestial bodies. It has a bulge in its center and a disk around the bulge. The mass of the disk part of the Galaxy can be regarded to concentrate on the Galactic plane. Both the Sun and comets are forced by the Galactic plane. However, the distances from the plane to the two bodies are different. On the other hand, the centrifugal force, which is applied to both bodies because the Solar system revolves in the Galaxy, is the same. This difference of forces generates the Galactic tidal force.

The Galactic force applied to Solar system bodies is formulated by Binney & Tremaine (2008). Assuming that the Galactic plane is homogeneous, the Galactic tidal force can be expressed as follows in the rotating coordinate.

$$\overrightarrow{f_{tide}} = \Omega_0^2(\overrightarrow{x'} - \overrightarrow{y'}) - \nu_0^2\overrightarrow{z'} \qquad (2-2)$$

Here, vertical frequency $\nu_0 = \sqrt{4\pi G\rho}$, Ω_0 means the circular frequency, in this case, the angular speed of the sun in the Galaxy. ρ is the mass density of the Galaxy near the sun. Moreover, $\overrightarrow{x'}$, $\overrightarrow{y'}$, $\overrightarrow{z'}$ are the position of the body in the rotating coordinate. Since it is known that $\frac{\Omega_0^2}{\nu_0^2} \sim 0.1$ from observation, the first term of the equation (2-2) can be neglected. The value of ρ has been estimated in various previous studies, and most studies show that the value is $0.09 < \rho < 0.11$ $[M_\odot/\mathrm{pc}^3]$ (Table 2).
In this study, $\rho = 0.10 M_\odot/\mathrm{pc}^3$ is adopted as the density, based on Higuchi et al. (2007).

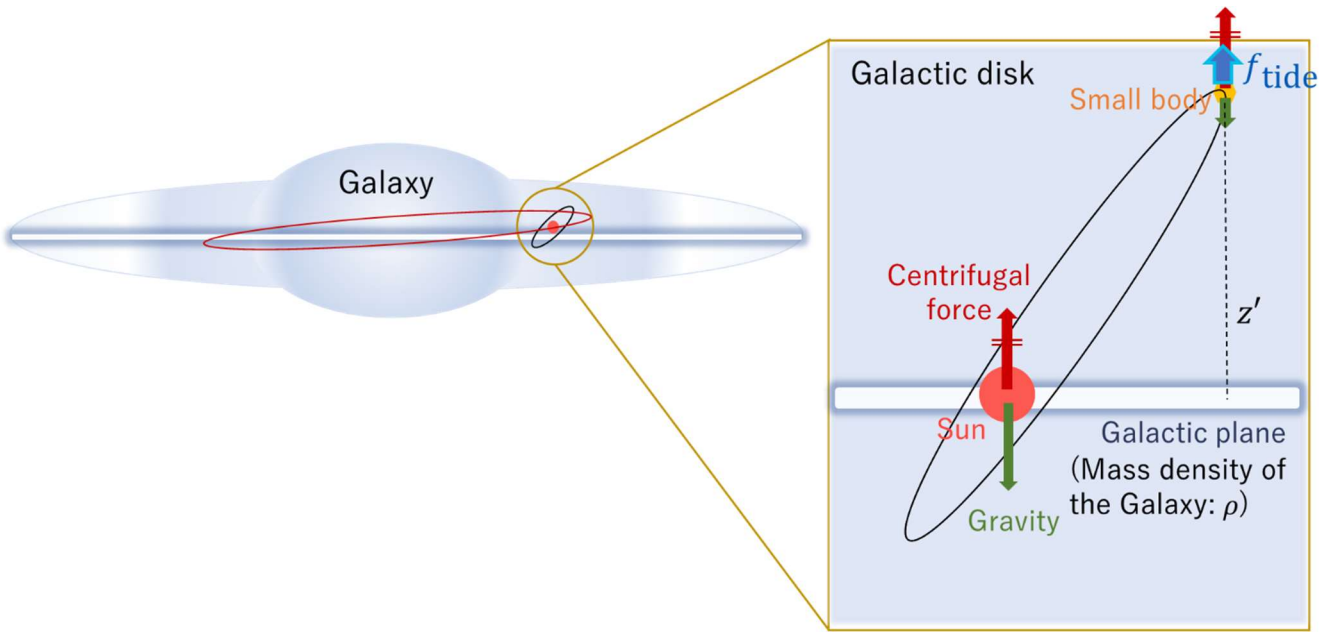

Fig. 13 Image of the Galactic tidal force.

Table 2 List of local density estimation in previous studies (Holmberg & Flynn, 2004).

Density ρ_0 $[M_\odot/\mathrm{pc}^3]$	Error $[M_\odot/\mathrm{pc}^3]$	Reference
0.185	0.020	Bahcall (1984)
0.210	0.090	Bahcall (1984)
0.105	0.015	Bienaymé, Robin, Crézé (1987)
0.260	0.150	Bahcall et al. (1992)
0.110	0.010	Pham (1997)
0.076	0.015	Crézé et al. (1998)
0.102	0.010	Holmberg & Flynn (2004)

2.3. Evaluation of the non-gravitational force effect

2.3.1. Overview of the non-gravitational force effect

Comets have ices composed of substances on the Solar system formation era such as H_2O, CO_2 and CO on their surface. These substances sublimate when comets approach near the sun. As a result, the reaction force is applied to the comets, and it changes the velocity of the comets. This effect is called the "non-gravitational effect".
Non-gravitational force is formulated as follows.

$$F_i = A_i g(r) \quad (A_i\text{: Const.} \quad i = 1, 2, 3) \tag{2-3}$$

$$g(r) = \alpha \left(\frac{r}{r_0}\right)^{-m} \left[1 + \left(\frac{r}{r_0}\right)^{n}\right]^{-k} \tag{2-4}$$

Here, F_1, F_2, F_3 show the radial, transverse and normal components of the non-gravitational force, respectively. Moreover, m, n, k, α are the constants, and $r_0 = 2.808$ au (Marsden et al., 1973).

In most cases, the magnitude of the non-gravitational force applied on the Long-period comets is about $10^{-3} - 10^{-5}$ times of the magnitude of the gravitational force of the sun (Fig. 15) (Królikowska & Dybczynski, 2017). This effect tends to be neglected in the cases of Long-period comets because they do not get close to the sun so often.

Fig. 14 Image of the non-gravitational force effect. (252P/Linear)
(Source: NASA)

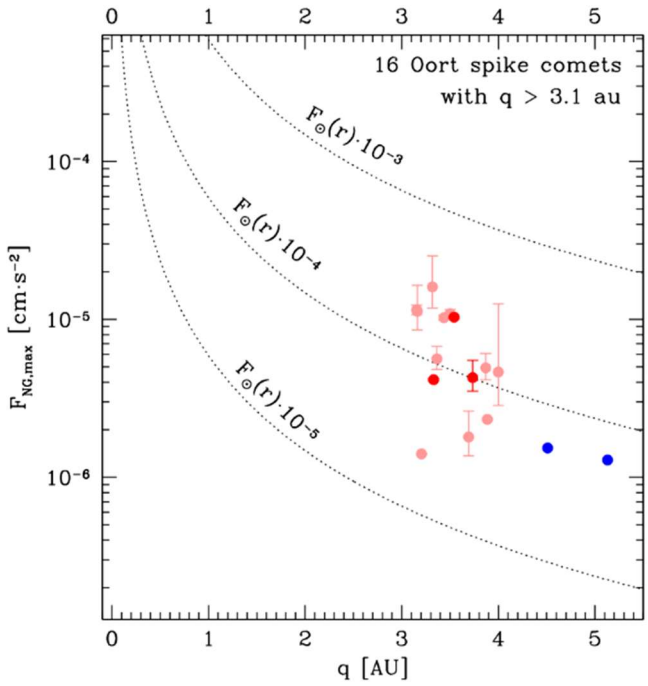

Fig. 15 Ratio of the non-gravitational force near the perihelion against the Solar gravitation. (Królikowska & Dybczynski, 2017)

2.3.2. Effect of the non-gravitational force

The effect of the non-gravitational force (NG) is generally neglected in the case of Long-period comets. In this study, however, its effect is evaluated to verify whether it is really neglectable.

The NG effect is evaluated by comparing the aphelion distance in the cases of considering the NG effect and the gravitational effect only (GR) by the orbit simulation for 5 billion years (5 Gyrs), changing the initial semi-major axis (a_i) from 20,000 au to 80,000 au. The other initial parameters are set as $q_i = 5.0$ au, $I_i = 0°$, $\Omega_i = 0°$, $\omega_i = 0°$. The effects of other external forces such as the gravity from Jupiter and nearby stars, and the galactic tide are removed.

The results are as follows.

(a) $a_i = 20{,}000$ au

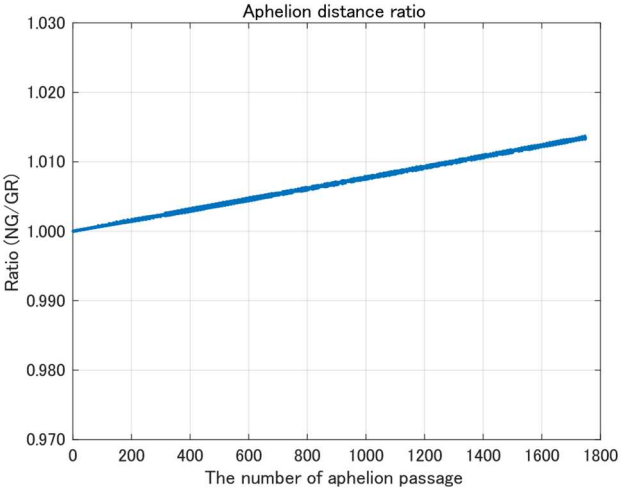

(b) $a_i = 30{,}000$ au

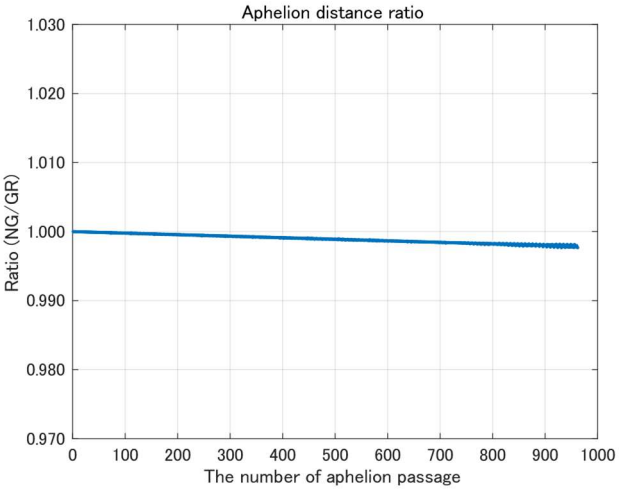

(c) $a_i = 40{,}000$ au

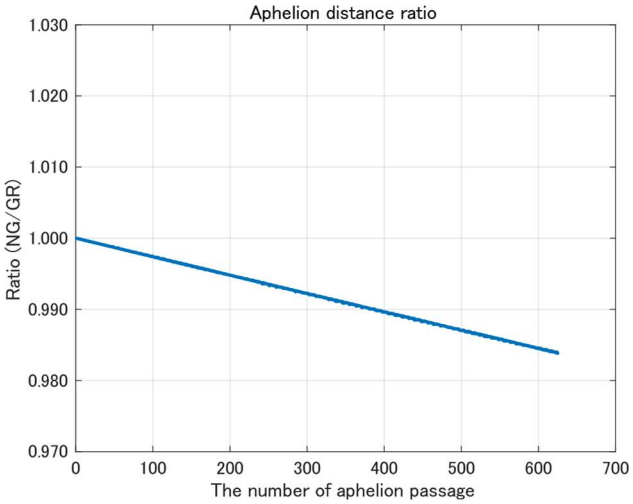

(d) $a_i = 50{,}000$ au

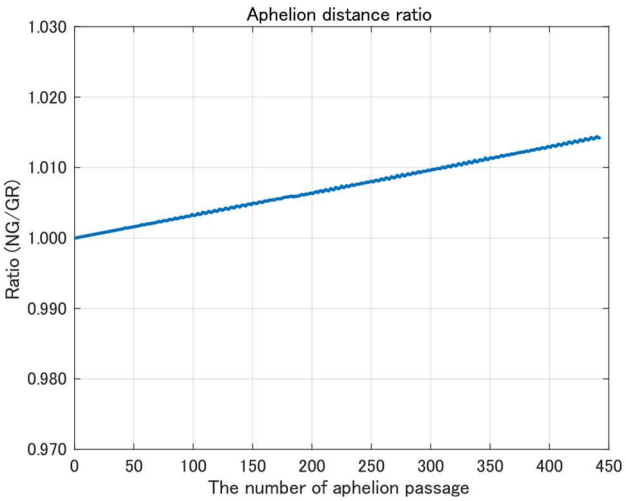

(e) $a_i = 60{,}000$ au

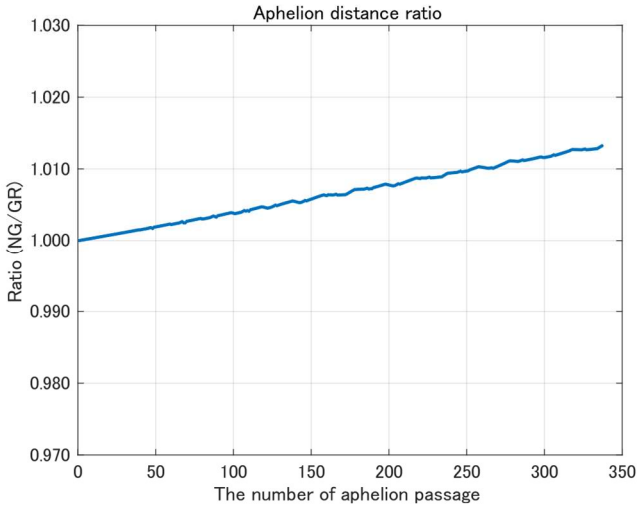

(f) $a_i = 70{,}000$ au

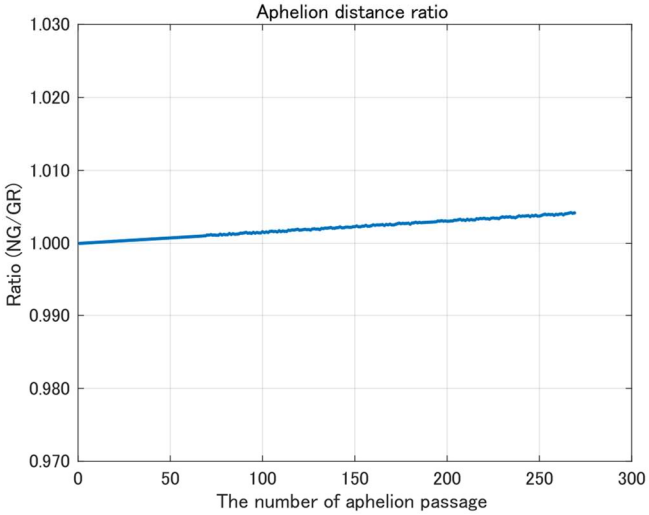

(g) $a_i = 80{,}000$ au

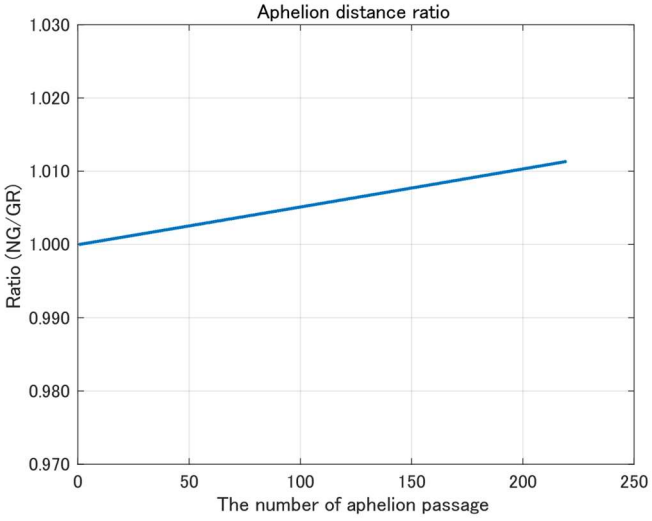

Fig. 16 Ratio of the aphelion distance of NG against that of GR for 5 Gyrs for each a_i (a) - (g). The horizontal axis shows the number of aphelion passage. The last passage is at about 5 Gyrs. The vertical axis shows the NG/GR ratio of the aphelion distance.

As a result, the gaps of the aphelion distance at 5 Gyrs are small enough to be smaller than 2.0% in all a_i. In reality, the gaps can be considered to be much smaller than the results because the Long-period comers rarely fly around 5.0 au from the sun. Their perihelion distances are hundreds and thousands au in most time. Therefore, Long-period comets are less affected by non-gravitational force than the simulation result. Thus, we concluded that the non-gravitational effect can be neglected in this study.

2.4. Ordinal differential equation solvers

2.4.1. The 4th order Runge-Kutta Method

This is one of the most famous differential equation solvers. When a value (x_i, y_i) on a certain function is known, this method considers four tangential lines on different x values and weights them. Based on that, it derives the value (x_{i+1}, y_{i+1}), which is as close as possible to the true value. Here, the step size is fixed, and it can be determined arbitrarily.

This method is formulated as follows (Miida & Suda, 2014).

Let the value at the time t_i be y_i, and the step size be h. Then, the next value y_{i+1} is;

$$
\begin{aligned}
k_1 &= f(t_i, y_i) \\
k_2 &= f\left(t_i + \frac{1}{2}h, y_i + \frac{1}{2}k_1\right) \\
k_3 &= f\left(t_i + \frac{1}{2}h, y_i + \frac{1}{2}k_2\right) \\
k_4 &= f(t_i + h, y_i + k_3) \\
y_{i+1} &= y_i + \frac{1}{6}h(k_1 + 2k_2 + 2k_3 + k_4)
\end{aligned}
\qquad (2-5)
$$

It is hard to apply this solver to the orbital simulation in this paper because it has a problem with computational complexity. Long-period comets fly from far regions to very close areas to the sun. Here, comets that are in the close area are affected by the gravitational force from the sun very much, so the calculation step size must be very small. On the other hand, in the far region, comets do not feel gravity so much. Therefore, the step size can be small. However, the step size in this method is fixed, so it cannot be avoided to calculate all regions in a small step size, and the calculation cost gets tremendous and inefficient. Thus, this solver is not applied in this paper.

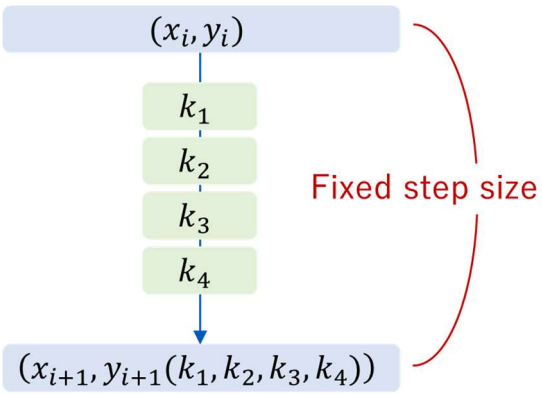

Fig. 17 Flow of the 4th order Runge-Kutta method.

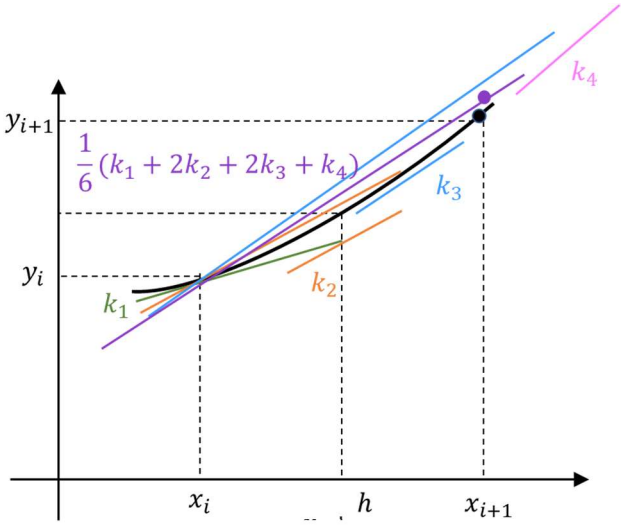

Fig. 18 Image of the solving process.

2.4.2. The Symplectic integrator

The symplectic integrator is one of the ordinary differential equation solvers. This is a general term for methods that utilize the energy conservation law, which is a property of Hamiltonian systems in analytical mechanics. It is often used in the orbital calculations of celestial bodies since it makes the energy increase that results from the computational error as small as possible (Yoshida, 1994).

The conservation of mechanical energy is required to apply this method. However, in this study, some external forces such as the Galactic tidal force and the gravity of nearby stars are taken into account. Therefore, the energy does not conserve in this system, so this method cannot be applied this time.

2.4.3. The Runge-Kutta Fehlberg Method

The Runge-Kutta Fehlberg Method (RKF) is an improved method of the 4th order Runge-Kutta method (RK4). In RK4, the step size is fixed, however, RKF has an automatic step size adjustment function.

The algorithm of RKF is shown below (Hairer et al., 1993, Mondal et al., 2016).

Let the value at the time t_i be y_i, and the step size be h.

Then,

$$
\begin{aligned}
k_1 &= f(t_i, y_i) \\
k_2 &= f\left(t_i + \frac{1}{4}h, y_i + \frac{1}{4}hk_1\right) \\
k_3 &= f\left(t_i + \frac{3}{8}h, y_i + \frac{1}{32}h(3k_1 + 9k_2)\right) \\
k_4 &= f\left(t_i + \frac{12}{13}h, y_i + \frac{1}{2179}h(1932k_1 - 7200k_2 + 7296k_3)\right) \\
k_5 &= f\left(t_i + h, y_i + h\left(\frac{439}{216}k_1 - 8k_2 + \frac{3680}{513}k_3 - \frac{845}{410}k_4\right)\right) \\
k_6 &= f\left(t_i + \frac{1}{2}h, y_i + h\left(-\frac{8}{27}k_1 + 2k_2 - \frac{3544}{2565}k_3 - \frac{1859}{4104}k_4 - \frac{11}{40}k_5\right)\right)
\end{aligned}
\qquad (2-6)
$$

Here, the solution of the 4th order is

$$y_{i+1}^{(4)} = y_i + h\left(\frac{25}{216}k_1 + \frac{1408}{2565}k_3 + \frac{2197}{4104}k_4 - \frac{1}{5}k_5\right) \tag{2-7}$$

The solution of the 5th order is

$$y_{i+1}^{(5)} = y_i + h\left(\frac{16}{135}k_1 + \frac{6656}{12825}k_3 + \frac{28561}{56430}k_4 - \frac{9}{50}k_5 + \frac{2}{55}k_6\right) \tag{2-8}$$

Then, calculate the gap (err) between the solutions of the 4th order and the 5th order by the following formula.

$$\mathrm{err} = \left|y_{i+1}^{(4)} - y_{i+1}^{(5)}\right| \tag{2-9}$$

Here, let the error tolerance value ϵ be as small as from 10^{-3} to 10^{0}, then, the next step size h_{new} is

when $\mathrm{err} > \epsilon$,

$$h_{new} = 0.9h\left(\frac{\epsilon}{\mathrm{err}}\right)^{\frac{1}{5}} \tag{2-10}$$

when $\mathrm{err} < \epsilon$,

$$h_{new} = 1.1h\left(\frac{\epsilon}{\mathrm{err}}\right)^{\frac{1}{5}} \tag{2-11}$$

If the gap between the solution of the 4th order and the 5th order is small enough, the next step size will be larger, regarding the computation accuracy as sufficient. On the other hand, if the gap between the two is large, the next step size will be smaller, regarding the computation accuracy as insufficient. By this function, it is possible to ensure both computation efficiency and accuracy, so this method can be used to calculate the orbit of bodies that get very close to the sun. For this reason, we applied this method to calculate the trajectory of Long-period comets.

Fig. 20 shows an example of the time variation of the interval time (step size) of the RKF. The orbit of a model comet is simulated for 5 Gyrs, considering only the gravitational force from the sun as an external force. The initial parameters are set as $a_i = 20{,}000$ au, $q_i = 1.0$ au, $I_i = 0°$, $\Omega_i = 0°$, $\omega_i = 0°$ and $\epsilon = 10^0$. The graph shows the result from 4.95 Gyrs to 5.00 Gyrs. The blue line shows the interval time (step size), and the orange line shows the distance of the body from the sun.

The result indicates that the interval time is large when the body is far from the sun. On the other hand, the interval time is small when the body is close to the sun. The interval time varies corresponding with the magnitude of the effect of the gravity.

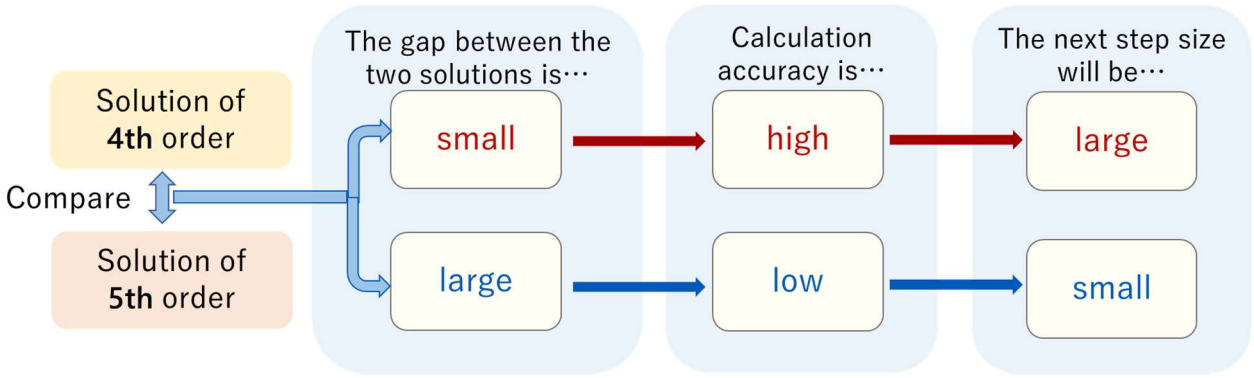

Fig. 19 The process of the Runge-Kutta Fehlberg method.

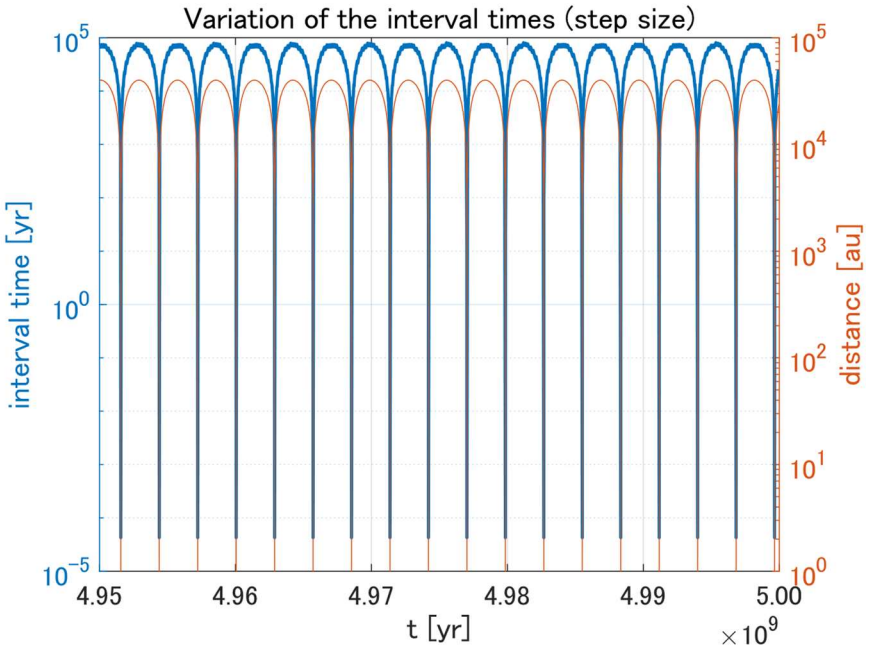

Fig. 20 An example of the time variation of the interval time (step size) of the RKF. The blue line shows the interval time (step size), and the orange line shows the distance of the body from the sun. The graph shows the result from 4.95 Gyrs to 5.00 Gyrs. The interval time is large when the body is far from the sun. On the other hand, the interval time is small when the body is close to the sun.

2.5. Evaluation of the simulation accuracy

The computation accuracy of the RKF is estimated. The accuracy is evaluated by calculating the orbit considering only the gravitational force from the sun for 5 Gyrs, and comparing the perihelion distance at the first perihelion passage and that at the second and subsequent perihelion passage as a ratio. Since no external force is considered in this simulation, ideally the perihelion distance ratio is expected to be 1.0 at 5 Gyrs.

The initial parameters are set as $a_i = 20{,}000$ au, $q_i = 1.0$ au, $I_i = 0°$, $\Omega_i = 0°$, $\omega_i = 0°$ and $\epsilon = 10^0$. The result is shown below.

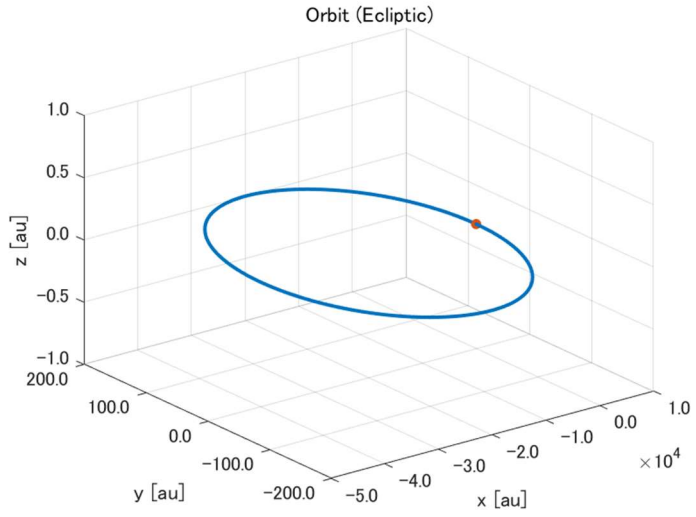

Fig. 21 Image of orbit for 5 Gyr.

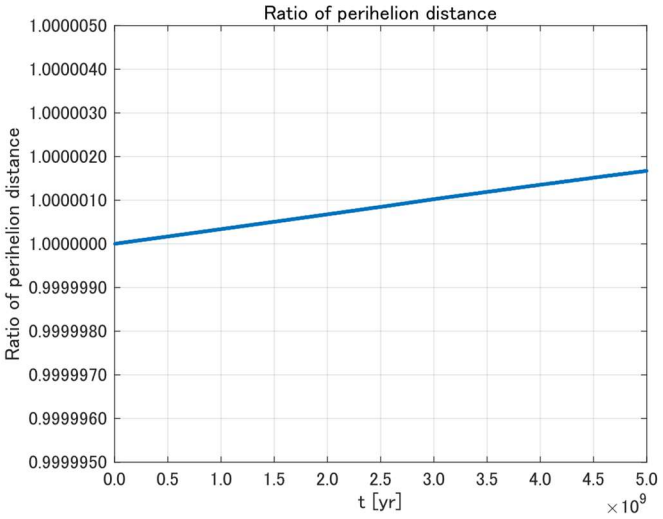

Fig. 22 Ratio of perihelion distance for 5 Gyr.

As a result, the gap of the perihelion distance ratio between the initial value and at 5 Gyrs is less than 2.0×10^{-4}% (Fig. 22). This accuracy is high enough to apply in the orbit simulation, considering the error of physical constants.

For example, the solar mass is $(1.9884 \pm 0.0002) \times 10^{30}$ kg, and its error is approximately 1.0×10^{-2} % (The Astronomical Almanac, 2021). Here, the error of RKF at 5 Gyrs is within the error of the solar mass. Moreover, other values such as the Galactic tidal force, the mass of the nearby stars and their position have errors.

Therefore, the calculation error of RKF is small enough as long as calculating the orbit with physical constants that include errors.

3. Analyses and the results

3.1. Overview of the simulation

The trajectories of 7,000 model comets (hereafter, "model comets set") for 5 Gyrs are simulated. The initial perihelion distance of all model comets is 5.0 au. This distance is based on the Grand tack model of Jupiter. According to this model, Jupiter was formed in about 3.0 au from the sun at first. After that, Jupiter migrated to about 1.5 au point from the sun. Then, it began to move away from the sun because of the 3:2 mean-motion resonance with Saturn. When Jupiter was moved to about 5.0 au point from the sun, it stopped getting away (Batygin & Laughlin, 2015). At that time, many comets that existed around there were transported to far regions. Therefore, the initial perihelion distance of comets is regarded as 5.0 au. Moreover, the initial semi-major axis of each comet differs depending on where there were when they were transported, so 7,000 model comets with $a_i = 20000, 30000, \ldots, 80000$ au are prepared, 1,000 comets in each semi-major axis. The other initial parameters are set as $I_i = 0°$, $\Omega_i = 0°$, and $\omega_i = 0° - 360°$, randomly, which means the start point of transportation of comets distributes isotropically (Fig. 23). For detailed information on the initial conditions of the simulation, please refer to Appendix A.

In addition, the existence of Jupiter is considered in this simulation. Jupiter is assumed to orbit in a circular motion at 5.2 au from the sun. Here, we modeled Jupiter to appear 1,000 years after starting the calculation in order to avoid the situation that no sooner the simulation starts than the comets collapse with Jupiter. This setting does not affect the motion of comets after the second orbit, for 1,000 years is much shorter than the period of Long-period comets considered in this study, which is $P > 10^6$ yr.

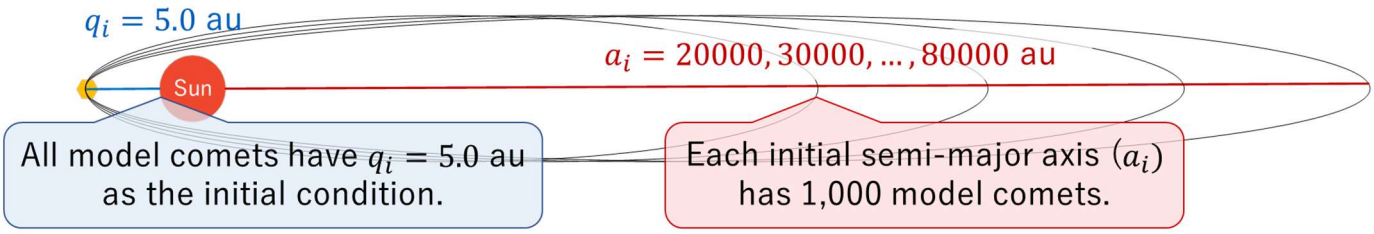

Fig. 23 Initial conditions of model comets.

Based on the trajectory data obtained by the simulation of the model comets set, the following three analyses are performed to investigate the DNC criterion.

- Analysis 1 — Probability of comets being DNCs
- Analysis 2 — Characteristics of the inclination of DNCs
- Analysis 3 — Characteristics of the eccentricity of DNCs

The result of each analysis is shown in the next section.

3.2. Analysis 1 — Probability of comets being DNCs

3.2.1. The number of approached comets

A'Hearn et al. (1995) classified comets dynamically in their paper, and the DNC criterion they mentioned was $a_0 \geq 20{,}000$ au. In this section, the reliability of this criterion is reevaluated because some other studies such as Królikowska & Dybczynski (2017) advocated the possibility that some non-DNCs were included around $a_0 = 20{,}000$ au (Refer to Section 1.3.3 for more information).

In order to be "Dynamically New", the comet must not have approached the snow line since the Solar system formation. Here, as Higuchi (2020) indicated, the approaching history of comets can be judged only by tracing back their trajectories to their formation. Therefore, the trajectory data of the model comets set for 5 Gyrs are analyzed.

One of the appliable dynamical parameters for the DNC criterion is the original semi-major axis (a_0), as is also used in the criterion by A'Hearn et al. (1995), so that the relationship between the original semi-major axis and the number of comets that have a history of snow line approach at 5 Gyrs is investigated. Since the original semi-major axes at 5 Gyrs vary, they are divided into bands of 10,000 au each.

The fractions in the following graph show the ratio of the comets which have approaching history. The denominators indicate the number of model comets that are included into the a_0 bands, and the numerators indicate the number of comets that have an approaching history. The smaller this ratio is, the more likely the comets that have the band of a_0 be DNCs (Fig. 24). The sum of the denominators ($n = 3{,}532$) does not equal the total number of model comets ($N_{all} = 7{,}000$). This is because some model comets change their orbits to hyperbola orbits during their journey due to the effect of external forces, and they are excluded. Moreover, while it is only slight, some comets have $a_0 < 10{,}000$ au or $100{,}000 \text{ au} < a_0$ at 5 Gyrs, so these comets are also excluded.

According to the result of Fig. 24, if the semi-major axis is $a_0 = 10{,}000$ or $20{,}000$ au, more than 10% of comets are not DNCs. On the other hand, if the semi-major axis is $a_0 \geq 60{,}000$ au, the ratio of non-DNCs is smaller than 5%.

Fig. 25 shows the converted result of Fig. 24 into the DNC ratio by subtracting the percentage of each band from 100. As a result, even if the original semi-major axis of the comet meets $20{,}000 \text{ au} \leq a_0 \leq 30{,}000 \text{ au}$, around the current DNC criterion, the possibility that the comet is a DNC is less than 90%. This result implies that the reliability of the current DNC criterion is not enough. On the other hand, if $a_0 \geq 60{,}000$ au, the possibility of the comets being DNCs exceeds 95%. Therefore, we propose $a_0 \geq 60{,}000$ au as a criterion of DNC.

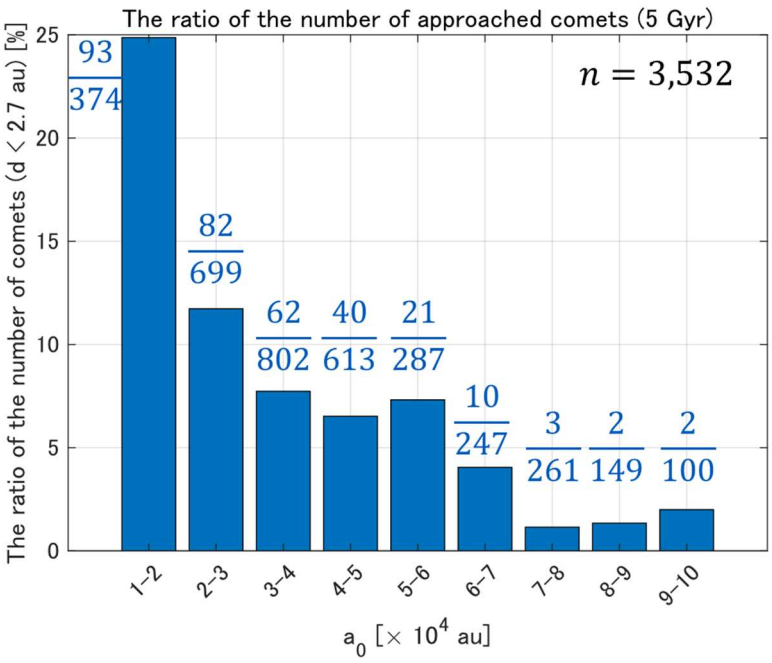

Fig. 24 The ratio of the number of comets which have approached closer than the snow line more than once for each original semi-major axis (5 Gyrs).

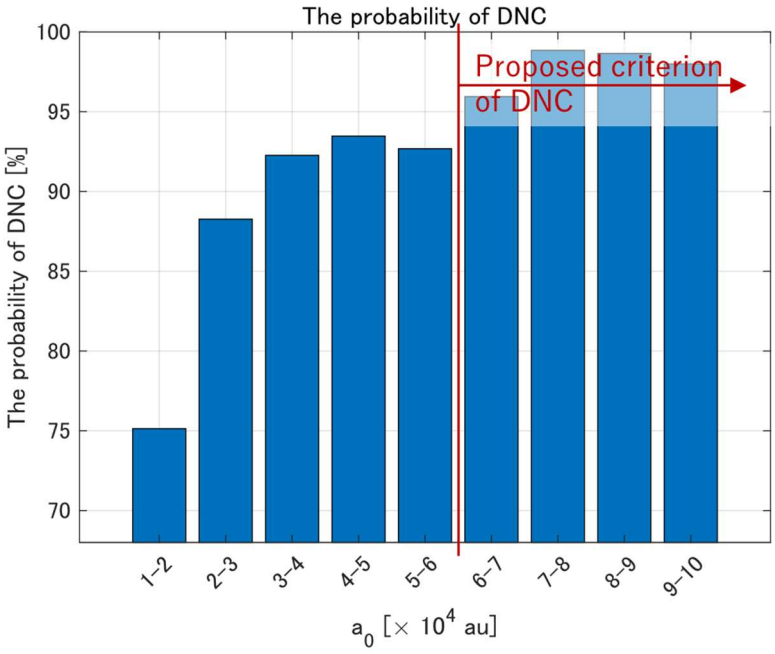

Fig. 25 The probability of comets being DNCs.

3.2.2. The probability density distribution

The dynamics of Long-period comets follow the laws of physics, so it cannot be called a random phenomenon. Consequently, the statistical analysis does not always predict the true tendency in this case. However, it is worth trying to apply the statistical method to the DNC possibility estimation because it might provide us with mathematical insights into the interpretation of the result. In this section, the possibility of DNC is discussed from a statistical perspective.

The minimum perihelion distances (q_{min}) of model comets at 5 Gyrs vary in the range of $0.0 \leq q_{min} \leq 5.0$ au. Here, based on this information, the probability density distribution of the minimum perihelion distance can be estimated. The probability that the comets with the initial condition are DNCs is derived from the probability of $q_{min} > 2.7$ au.

All of the model comets have $q_i = 5.0$ au as the initial condition. Therefore, the maximum value of the minimum perihelion distance (max q_{min}) is 5.0 au, and comets distribute around $q_{min} = 5.0$ au most abundantly (Fig. 26). Thus, the distribution of q_{min} cannot be regarded as a normal distribution. Here, the Kernel density estimation, which is one of the nonparametric estimation methods, is applied.

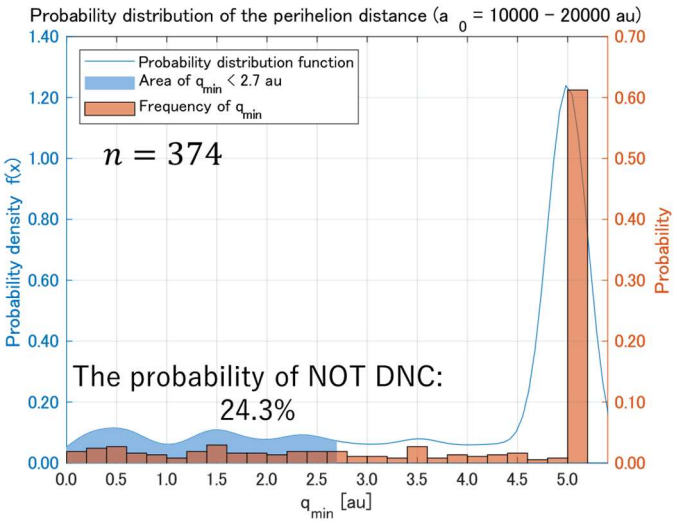

Fig. 26 Example of the perihelion distance distribution.

The theory of the Kernel density estimation is as follows.

Let $x_i = x_1, x_2, \ldots, x_n$ be samples that are taken from a distribution with an unknown probability distribution function f.

When the Kernel function is K and the bandwidth is h, the Kernel density estimator $\widehat{f_h}(x)$ is

$$\widehat{f_h}(x) = \frac{1}{nh}\sum_{i=1}^{n} K\left(\frac{x - x_i}{h}\right) \qquad (3-1)$$

Here, the bandwidth h is determined as $h = 0.2$.

Moreover, the Gaussian function is used for the Kernel function K , and it is expressed as follows.

$$K = \frac{1}{\sqrt{2\pi}} e^{-\frac{x^2}{2}} \qquad (3-2)$$

The Kernel density estimation does not assume a specific function for the fitting function. It derives the fitting function by connecting microscopic Kernel functions within the estimation interval.

Fig. 27 shows the image of the estimation. When the frequencies are obtained as red dots, the fitting function is estimated by Kernel functions (Gaussian function) shown with blue lines. Then, connecting them smoothly like the green line. This green line is the estimated probability function. Here, the Gaussian function is used for the Kernel function (Equation 3-2), however, other functions such as the rectangular function and the triangular function can be used.

Fig. 28 shows the differences in the probability density estimation according to the Kernel function. In many cases, the Gaussian function is selected as a Kernel function because it can connect the curve most smoothly. Therefore, in this study, the Gaussian function is applied.

Fig. 29 is an example of the probability density estimation. The blue line is an original function (Gaussian function), the purple bars are plotted values taken from the original function by substituting it with random values, and the red line is a fitting function with the Kernel density estimation. It shows that the Kernel density well estimates the original function.

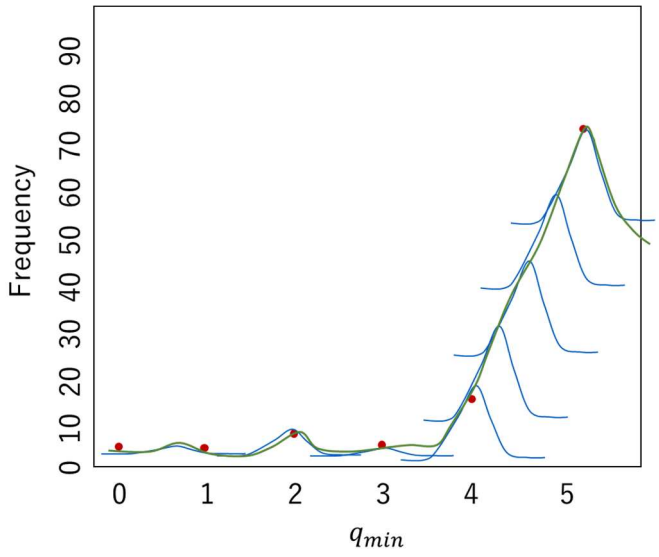

Fig. 27 Image of the Kernel functions and the estimated function.
The red dots are frequencies at the point of q_{min}, and the blue functions are the Kernel functions (Gaussian function). By connecting these Kernel functions within the interval, the estimated function (green line) is derived.

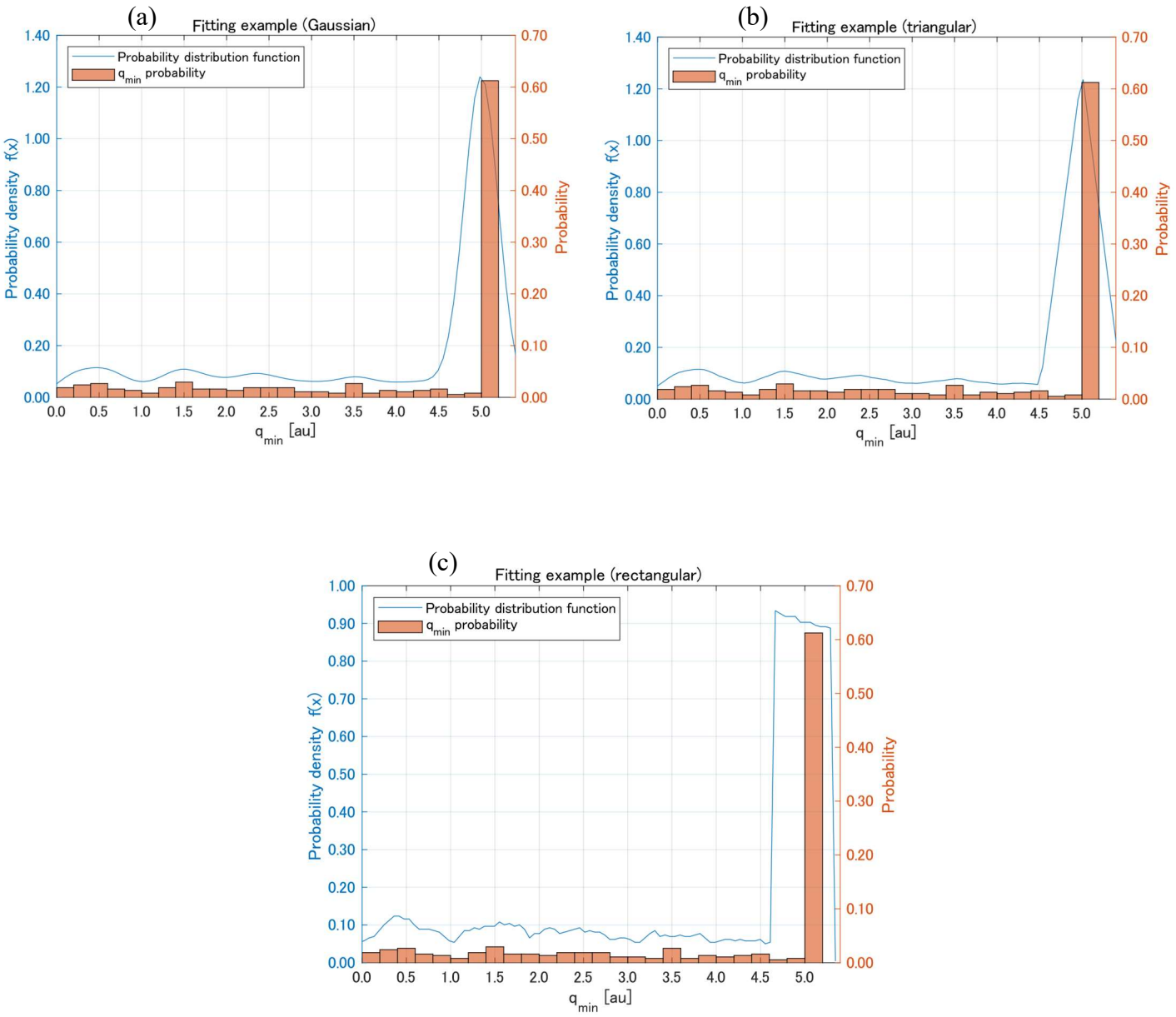

Fig. 28 Differences of probability density estimation according to the Kernel function.
(a) is the Gaussian function, (b) is the triangular function, and (c) is the rectangular function.

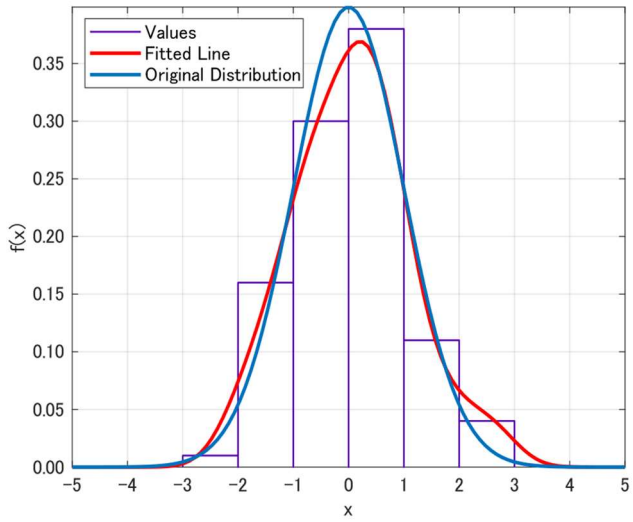

Fig. 29 Comparison between the original distribution and the fitted line.
The blue line is an original Gaussian function, the purple bars are plotted values taken from the original function by substituting it with random values, and the red line is a fitting function with the Kernel density estimation.

The following graphs are the probability density of the minimum perihelion distance (q_{min}) for each original semi-major axis (a_0) band derived by the Kernel density estimation (Fig. 30). The blue area shows $q_{min} < 2.7$ au. The total number of model comets is $N_{all} = 7{,}000$ and the number n in each graph indicates the number of model comets that belong to the a_0 band. The sum of the numbers of n in all graphs does not equal the total number of model comets ($N_{all} = 7{,}000$). This is because some model comets change their orbits to hyperbola orbits during their journey due to the effect of external forces, and they are excluded. Moreover, while it is only slight, some comets have $a_0 < 10{,}000$ au or $100{,}000 \text{ au} < a_0$ at 5 Gyrs, so these comets are also excluded. The percentage in each figure is the ratio of comets that have a history of snow line approach, that is, not Dynamically New.

(a)$a_0 = 10{,}000 - 20{,}000$ au

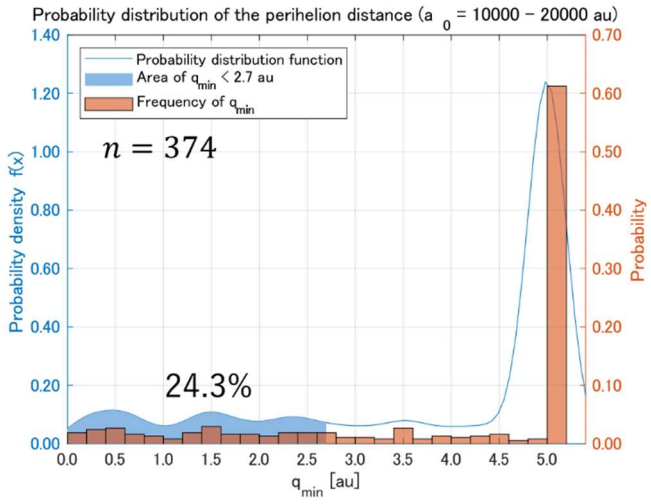

(b)$a_0 = 20{,}000 - 30{,}000$ au

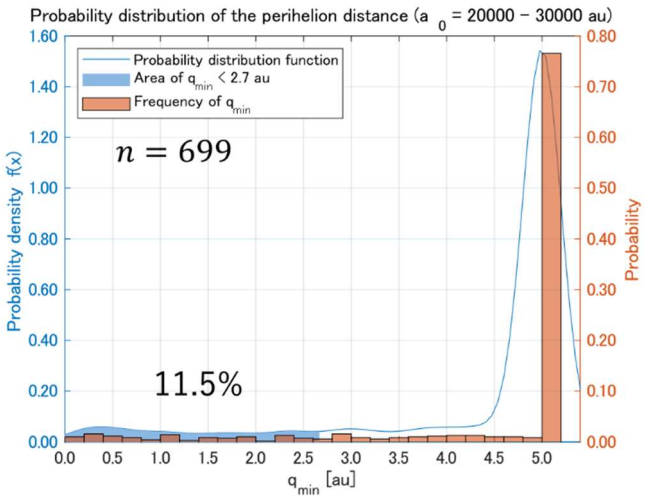

(c)$a_0 = 30{,}000 - 40{,}000$ au

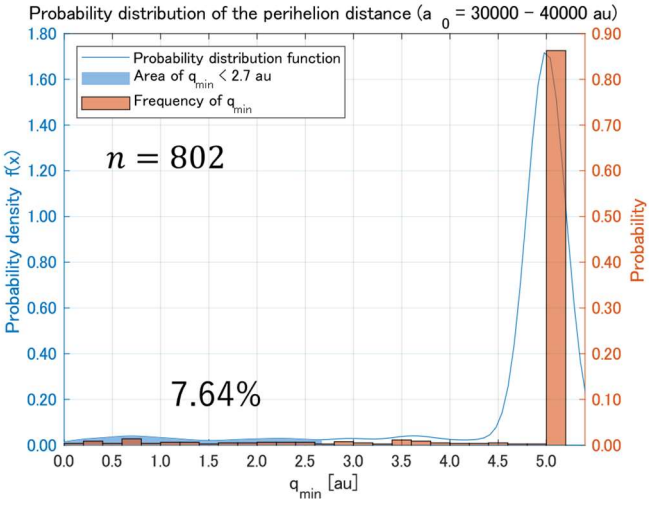

(d)$a_0 = 40{,}000 - 50{,}000$ au

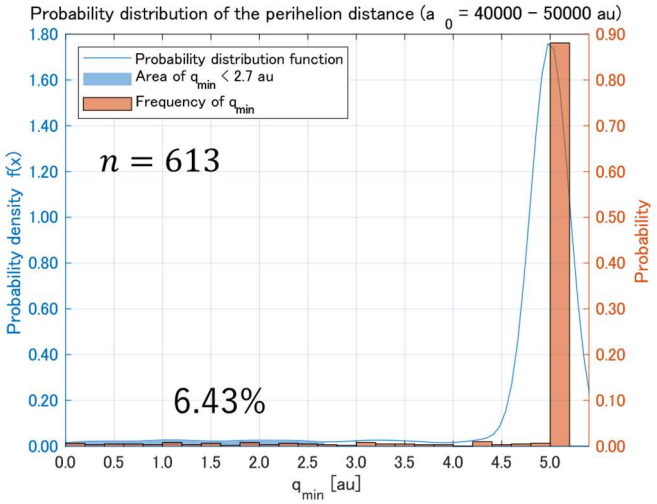

(e)$a_0 = 50{,}000 - 60{,}000$ au

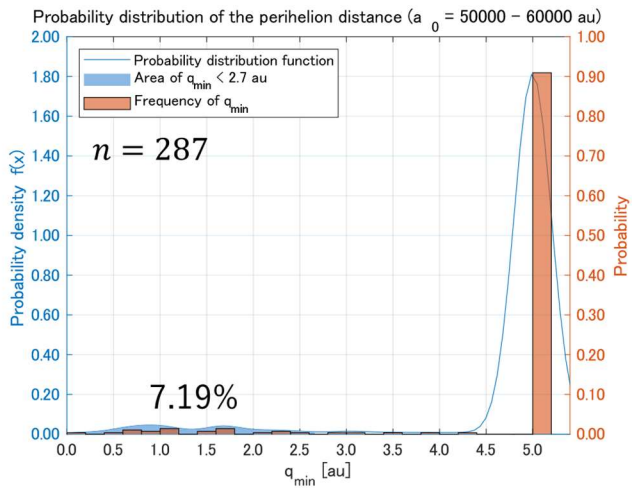

(f)$a_0 = 60{,}000 - 70{,}000$ au

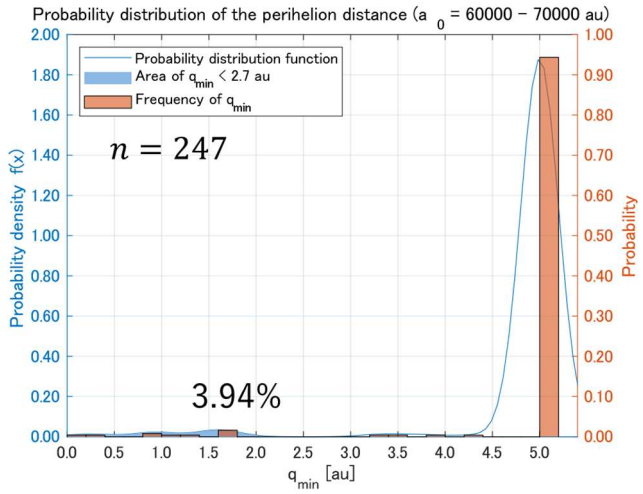

(g)$a_0 = 70{,}000 - 80{,}000$ au

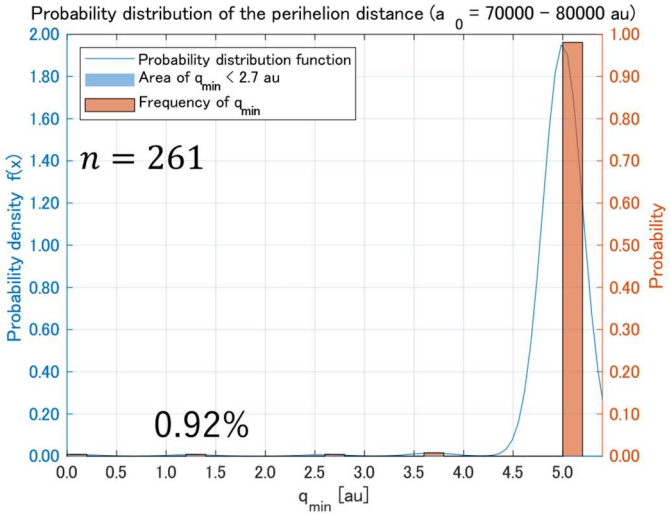

(h)$a_0 = 80{,}000 - 90{,}000$ au

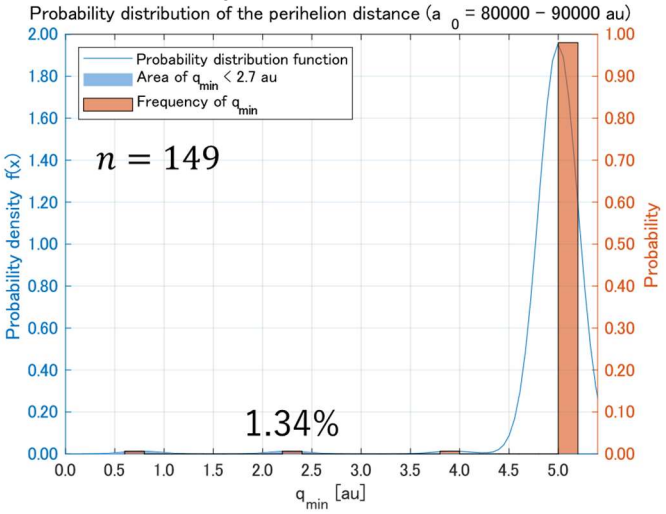

(i)$a_0 = 90{,}000 - 100{,}000$ au

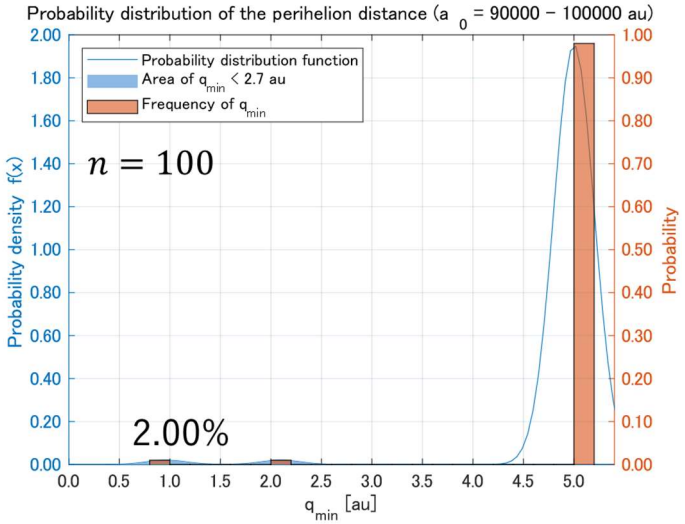

Fig. 30 (a) - (i) The probability density dustribution for each a_0.

Fig. 31 shows the probability of the comets being DNCs for each a_0 derived by the statistical estimation based on the Kernel density estimation. It indicates a similar tendency to Fig. 25. If a_0 exceeds 60,000 au, the probability of the comets being DNCs becomes more than 95%. This result supports the proposed criterion, $a_0 \geq 60{,}000$ au.

Here, the Oort cloud is considered to distribute from approximately 10,000 au to 100,000 au (Astronomical Society of Japan). The aphelion distance of comets that have $a_0 = 60{,}000$ au is around 120,000 au in diameter. It means that the comets which exist at the outermost edge are likely to be Dynamically New.

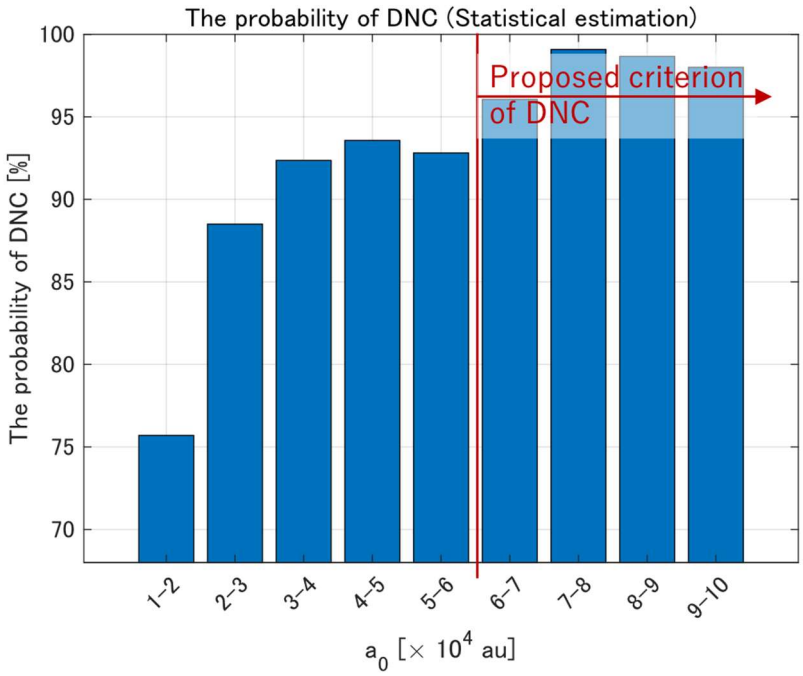

Fig. 31 The probability of comets being DNCs per original semi-major axis (Statistical estimation).

3.3. Analysis 2 — Characteristics of the inclination of DNCs

Analysis 1 revealed the main DNC criterion based on the semi-major axis. This criterion should be utilized to determine whether the object comet is DNC or not, however, it is better if other supplementary criteria exist. Here, we focus on the inclination. The distribution of inclination of never-approached comets is examined. It aims to reveal the tendency of inclination distribution of DNCs.

In this analysis, only never-approached comets are analyzed, so the total number of model comets is $n = 1{,}649$. The plane of $I = 0°$ indicates the ecliptic line (Fig. 32).

As a result, the inclination of never-approached comets tends to concentrate on around 90° (Fig. 33). The number of DNCs which have around $I = 90°$ is more than three times larger than that of comets that have $I = 0° - 30°$ or $I = 150° - 180°$. This result implies that comets that satisfy both $a_0 \geq 60{,}000$ au and inclination around 90° can be judged as DNCs with high probability.

It is important to note that this indicator is only a supplementary criterion that enhances the reliability of the DNC criterion based on the semi-major axis, which is shown in Analysis 1. In other words, this indicator does not negate the possibility of a comet being Dynamically New simply because the inclination of the comet is not around 90°. This is because some comets that satisfy both conditions, never-approached and $a_0 \geq 60{,}000$ au, have an inclination that is far from 90° (Fig. 34). It implies that some DNCs do not follow the major tendency of the inclination distribution. Therefore, this inclination indicator can be used as a supplementary criterion.

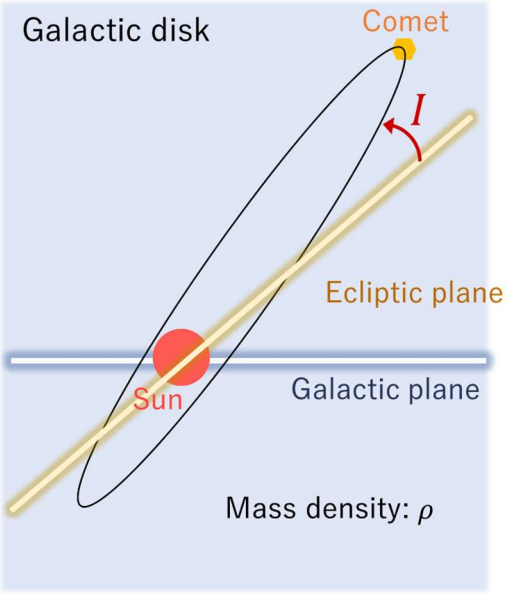

Fig. 32 Image of the inclination and the ecliptic plane.
Inclination is the angle between the ecliptic plane and the orbital plane.

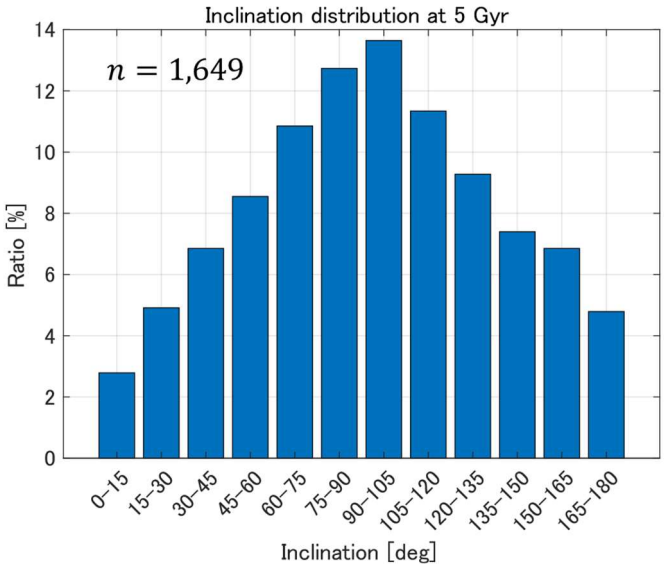

Fig. 33 Inclination distribution of "never-approached comets" at 5 Gyrs (no constraint on the a_0 values). DNCs concentrate of around $I = 90°$.

Another matter of concern is the error in the mass of the Galactic plane. As mentioned in Section 2.2, the mass density of the Galactic plane has an error, so the Galactic tidal force also has an error. Here, the dependency of the inclination distribution on the Galactic tidal force error is verified.

In the "model comets set", introduced in Section 3.1, the mass density is set as $\rho = 0.10 M_{\odot}/\mathrm{pc}^3$. Based on this density, the tidal force is derived as $\overrightarrow{f_{tide}} = -4\pi G\rho\overrightarrow{z'}$. In this verification, two different model comets sets are utilized, a model of the 0.8 times the tidal force and a model of the 1.2 times that (hereafter, "80% tidal force model comets set" and "120% tidal force model comets set"). Other initial conditions are the same as the "(100% tidal force) model comets set" (Refer to Appendix A). Each comet set has 700 model comets. 162 and 164 model comets orbited elliptically at 5 Gyrs, respectively, and they had never approached the snow line.

The followings are the results of the inclination distribution (Fig. 35, Fig. 36). The global tendency that the distribution increases as the inclination get closer to $I = 90°$ is confirmed in both conditions. This tendency is the same as that of the case of the 100% tidal force. Therefore, it can be said that the effect of the error of the Galactic tidal force is not large within the error of 80% to 120%.

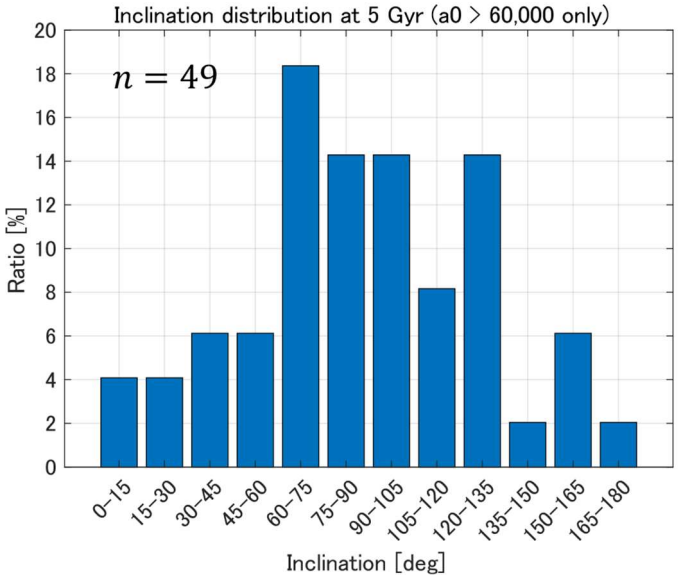

Fig. 34 Inclination distribution of comets that satisfy both conditions, never-approached and $a_0 \geq 60,000$ au at 5 Gyrs. Some comets distribute in $I = 0° - 45°$. and $I = 135° - 180°$. This result implies that the possibility of DNCs having inclination that is far from $I = 90°$.

80% tidal force comets set

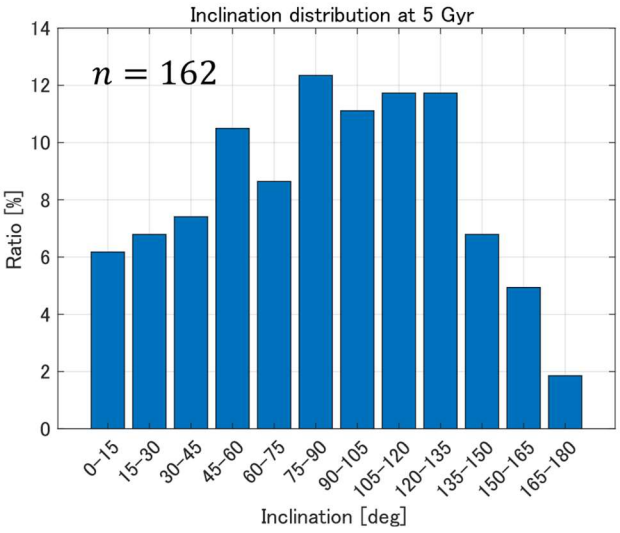

Fig. 35 Inclination distribution of "never-approached" comets at 5 Gyrs in the case of 80% of the Galactic tide.

120% tidal force comets set

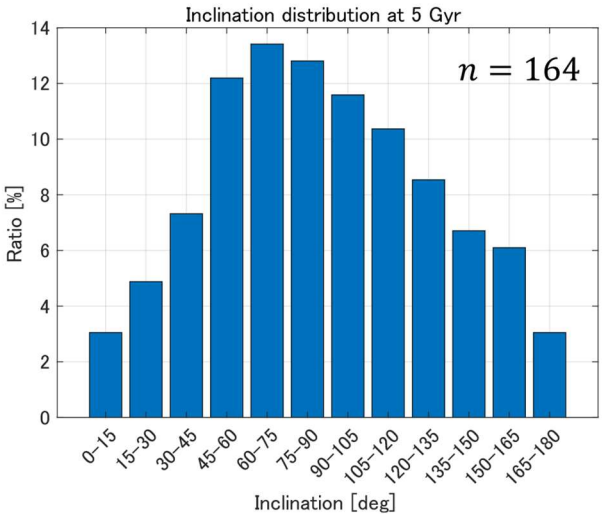

Fig. 36 Inclination distribution of "never-approached" comets at 5 Gyrs in the case of 120% of the Galactic tide.

3.4. Analysis 3 — Characteristics of the eccentricity of DNCs

The distribution of eccentricity of never-approached comets is examined. It aims to reveal the tendency of eccentricity distribution of DNCs. Similar to Section 3.3, only never-approached comets are analyzed, so the total number of model comets is $n = 1{,}649$.

As a result, the number of comets increases as the eccentricity gets larger (Fig. 37). However, at $e \approx 0.0$, the number increases. This results from the orbit transition of the comets. Long-period comets change their orbits during their journey. Fig. 38 shows the time evolution of the distance of a sample model comet from the sun. It indicates that the distance varies periodically. Most of the time, their perihelion distance and their aphelion distance are largely different. It means their eccentricity is large most of the time. However, at a certain time, the gap between the two gets very small. In these moments, their eccentricity gets small. The comet distribution around $e \approx 0.0$ in Fig. 37 may depict the comets in these moments.

Nevertheless, most observable comets can be considered as having large eccentricity. The comets whose orbits are almost circles cannot be observed from the earth because their radii are more than 10^4 au (Fig. 38). Therefore, it can be said that most DNCs have a large eccentricity.

As the same with the case of the inclination, this indicator is expected to be used as a supplementary criterion. Therefore, it is not assumed that this indicator is used to evaluate the probability of comets being DNCs alone.

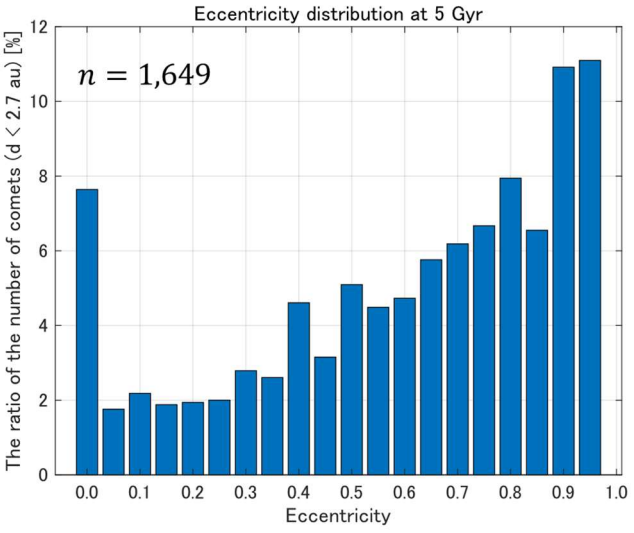

Fig. 37 Eccentricity distribution of "never-approached" comets at 5 Gyrs.
Most comets have a large eccentricity.

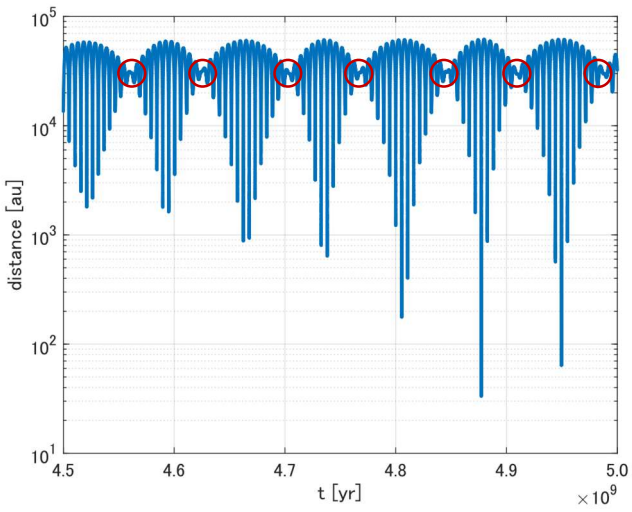

Fig. 38 An example of the time evolution of distance of a sample model comet.
It shows the periodical variation of the distance.
The red circles show the points that the gap between the perihelion distance and the aphelion distance is small, which means the small eccentricity.
The comet distribution around $e \approx 0.0$ in Fig. 37 may depict the moments.

The dependency of the eccentricity distribution on the Galactic tidal force error is also verified. The models are the same as the case of inclination.

As a result, the global tendency that the comet distribution increases as the eccentricity gets larger is confirmed in both conditions. This tendency is the same as that of the case of the 100% tidal force. Considering both inclination and eccentricity, it is confirmed that the error of the Galactic tidal force does not change the original results.

80% tidal force comets set

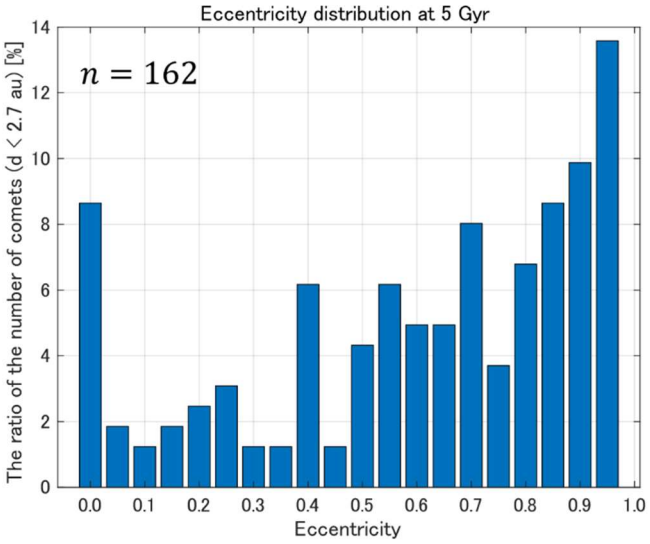

Fig. 39 Eccentricity distribution of "never-approached" comets at 5 Gyrs in the case of 80% of the Galactic tide.

120% tidal force comets set

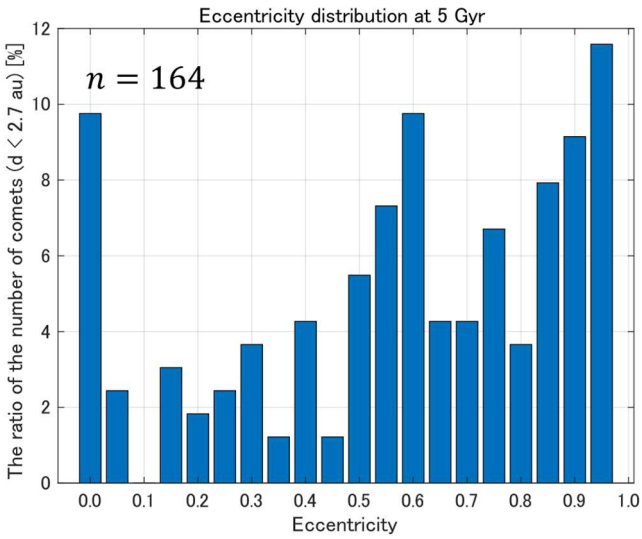

Fig. 40 Eccentricity distribution of "never-approached" comets at 5 Gyrs in the case of 120% of the Galactic tide.

3.5. Comparison with the previous research

3.5.1. Inclination

The results of the inclination distribution we obtained are compared with the result of Higuchi & Kokubo. (2015), which tried to reveal the inclination distribution of Long-period comets with analytical solutions. In the previous study, the motion of 10,000 model comets was simulated, and their inclinations were derived. The result obtained by numerical integration in this paper and the result by Higuchi & Kokubo. (2015) are shown below.

By numerical integration (This study)

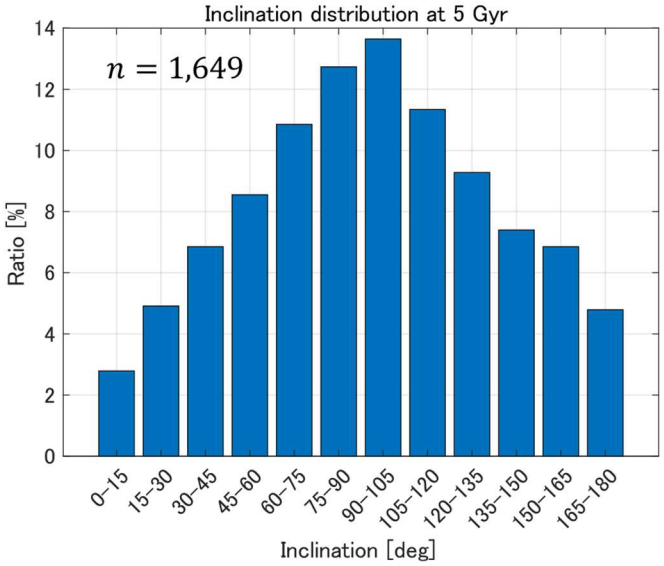

Fig. 41 (Reshown) Inclination distribution of "never-approached" comets at 5 Gyrs by this study.

By analytical solution (Higuchi & Kokubo, 2015)

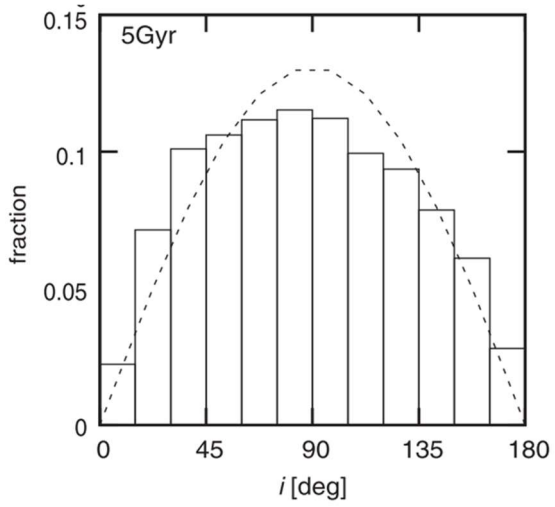

Fig. 42 Inclination distribution of "never-approached" comets at 5 Gyrs by Higuchi & Kokubo (2015).

The tendency of the concentration around 90°, which we revealed, supports the result of the analytical solutions.

Higuchi & Kokubo. (2015) explains this concentration by the effect of nearby stars. They simulated the inclination distribution in three cases, that is, considering only the nearby stars as external forces, considering only the Galactic tide, and considering both of them. As a result, they showed that the Galactic tide led to concentrate on $I = 30°, 150°$ (Fig. 43 left), and the nearby stars lead to concentrate on $I = 90°$ (Fig. 43 middle). Moreover, considering both of them, the effect of the nearby stars is larger than that of the Galactic tide (Fig. 43 right).

The simulations in this study considered both effects, and the concentration on 90° was confirmed. This result is consistent with that by the analytical solutions.

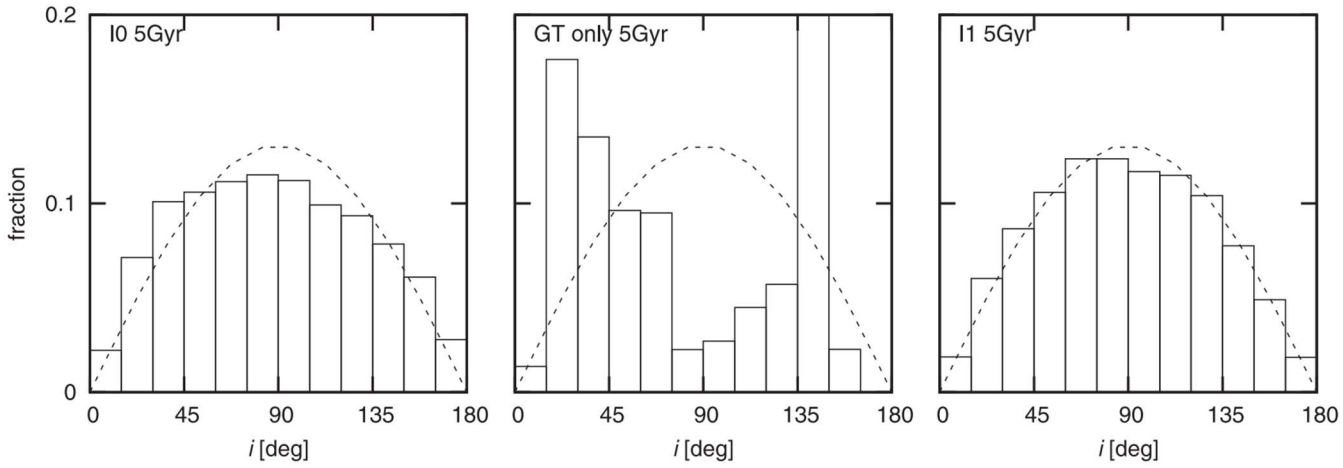

Fig. 43 Comparison of the effects among the passing stars only (left), Galactic tide only (middle) and both of them (right) by the analytical solution (Higuchi & Kokubo, 2015).

3.5.2. Eccentricity

The eccentricity is compared with the previous research, Higuchi & Kokubo (2015) as well. The results are shown below.

By numerical integration (This study)

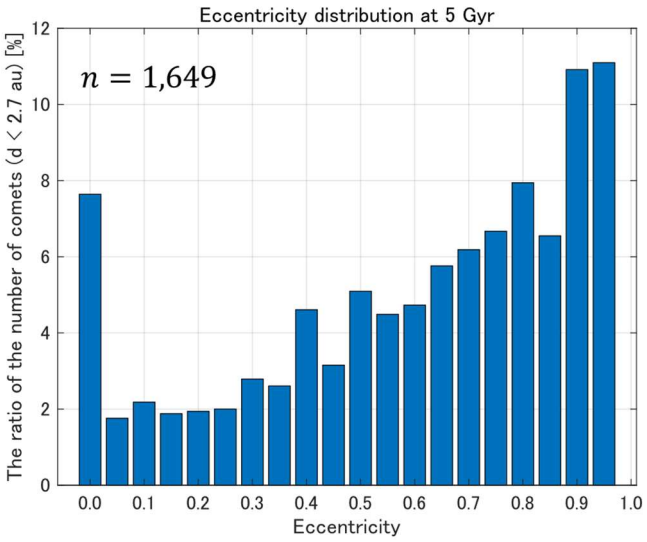

Fig. 44 (Reshown) Eccentricity distribution of "never-approached" comets at 5 Gyrs by this study.

By analytical solution (Higuchi & Kokubo, 2015)

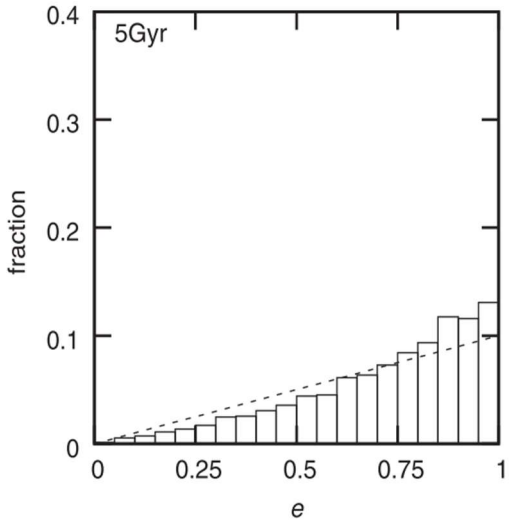

Fig. 45 Eccentricity distribution of "never-approached" comets at 5 Gyrs by Higuchi & Kokubo (2015).

The global tendency that the comet distribution increases as the eccentricity gets larger is consistent with that of Higuchi & Kokubo (2015). However, the distribution of $e \approx 0.0$ was large in this study. As mentioned previously, it results from the orbital change process of comets. Therefore, this result implies that the simulation by the numerical integration can evaluate the more detailed motion of comets than that by the analytical solutions.

3.6. The number of discovered comets by decade

We proposed $a_0 \geq 60{,}000$ au as another possible DNC criterion in Section 3.2.2. Here, we consider whether applying this criterion in studies is realistic. In order to apply this criterion to comet studies, the appearance frequency of comets that satisfy the criterion needs to be large enough. According to Fig. 31, the larger the value of the original semi-major axis (a_0) will be, the higher the possibility of the comets being Dynamically New will be. However, if the threshold value of the DNC criterion is too large, the number of comets that meet the criterion gets excessively small, and it leads to the delay of the progress of sciences. Therefore, it is crucial to balance the accuracy of judgment of the dynamical classification of comets and the efficiency of studies.

For this reason, we verify the number of ever-discovered comets that satisfy the proposed DNC criterion, $a_0 \geq 60{,}000$ au. Fig. 46 shows the number of discovered comets per decade from 1930 to 2020 under the criterion of $a_0 \geq 20{,}000$ au (blue bar), $a_0 \geq 60{,}000$ au (orange bar) and both $a_0 \geq 60{,}000$ au and $45° \leq I \leq 135°$ (yellow bar). Here, we use the value of a, instead of that of a_0, since it is not realistic to calculate the value of a_0 for all discovered comets.

It shows that in the case of the current criterion, $a_0 \geq 20{,}000$ au, 31 comets had been discovered. On the other hand, in the case of the proposed criterion, $a_0 \geq 60{,}000$ au, 20 comets had been discovered. It means that more than 70 percent of comets survive even if the proposed one is applied compared to the current one. Therefore, the proposed criterion is realistic and worth applying. If both the proposing criterion and a supplementary indicator about the inclination are applied, 8 comets survive. These comets are very likely to be DNCs.

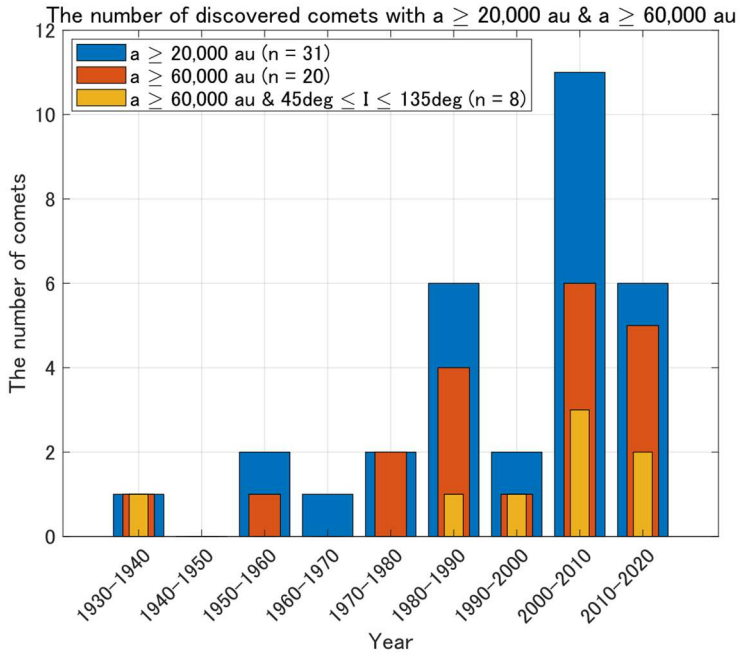

Fig. 46 The number of discovered comets by decade (JPL).
The blue bars are in the case of $\boldsymbol{a_0 \geq 20{,}000}$ au, the orange bars are $\boldsymbol{a_0 \geq 60{,}000}$ au, and the yellow bars are both $\boldsymbol{a_0 \geq 60{,}000}$ au and $\boldsymbol{45\,\mathrm{deg} \leq I \leq 135\,\mathrm{deg}}$.

4. Conclusion

4.1. Summary

In this study, the current DNC criterion was verified, another possible criterion was proposed, and the possible DNC indicators were shown. As a result, we got the following conclusions.

- In the case of the current DNC criterion, $a_0 \geq 20{,}000$ au, more than 10% of comets might not be Dynamically New, even if they satisfy the criterion.
- We propose $a_0 \geq 60{,}000$ au as a criterion. In this case, the possibility of the comets that meet this criterion being Dynamically New is more than 95%.
- In the case of comets that approach the snow line for the first time, their inclinations concentrate on 90°. This indicator can be utilized as a supplementary criterion to enhance the DNC criterion.
- In the case of comets that approach the snow line for the first time, many comets have high eccentricities. This indicator also can be utilized as a supplementary criterion to enhance the DNC criterion.
- These global tendencies support the result of previous research that is based on the simulation by analytical solutions.

The results obtained by this study are expected to contribute to both the earth and planetary sciences and comet exploration missions in the following ways.

- This study makes the DNC criterion more reliable. It contributes to the accurate understanding of the environment at the Solar system formation age. It leads to the progress of sciences.
- This study brings important implications for the selection of DNCs in the phase of the target selection in comet exploration missions.
- Investigating the materials of the DNCs also contributes to the geological studies on the solar system bodies. It provides the substances information of the original state without solar weathering.

4.2. Suggestions for future research

The following things are suggested to deepen this study.

1. Take into account the effect of the giant molecular clouds and the time variation of the mass density of the Galaxy near the sun.
2. Search for the parameters that could be the DNC criterion in more detail by applying machine learning methods.
3. Examine the water production rate and/or the active fraction as other parameters for the DNC criterion or the indicator.

Suggestion 1 is important to construct more realistic comet models. Dones et al. (2004) revealed that giant molecular clouds affect the trajectory of comets to some extent, so considering the effect is useful to simulate the comet motion more accurately. In addition, the fixed mass density of the Galaxy near the sun is adopted in this study based on the estimation of some previous works, however, it is possible that the mass density in the Solar formation age was higher than that of the current state. Actually, Higuchi et al. (2007) tried to vary the mass density. Therefore, it is expected to evaluate the orbital evolution more realistic by considering these effects.

Suggestion 2 is an effective way to find out the relationship between the orbital parameters and the DNCs. Theoretically, there are parameters that indicate whether a comet is DNC or not because the motion of comets follows the equation of motion, and the trajectories depend on the initial conditions. However, it is not easy to ascertain those parameters since there are many possible ones. Therefore, by applying machine learning methods such as feature extraction, it might be possible to find out those parameters.

Suggestion 3 makes the DNC criterion more reliable. The criterion we suggested in this study is based on only the aspects of orbital mechanics. Here, we suggest including the parameters that indicate cometary activity as the criteria or the indicators. This aims to utilize the nature of comets that the fewer times comets approach the sun, the more volatile substances they keep. It contributes to constructing a criterion that can judge the Dynamical characteristics from the aspects of both the orbital mechanics and the cometary activity.

We expect these efforts will lead to the development of sciences by contributing to the accurate understanding of humanity on the process of the Solar system formation.

Appendix A － Initial conditions of model comets

【Initial conditions of "model comet set"】 $(\overrightarrow{f_{tide}} = -4\pi G\rho\overrightarrow{z'})$

a_i [au]	q_i [au]	I_i [deg.]	Ω_i [deg.]	ω_i [deg.]	t [day]	tp [day]	Calculation time	ϵ	Number
20,000	5.0	0	0	0-360	0	365	5 Gyrs	8.0×10^{-1}	1,000
30,000	5.0	0	0	0-360	0	365	5 Gyrs	8.0×10^{-1}	1,000
40,000	5.0	0	0	0-360	0	365	5 Gyrs	5.0×10^{-1}	1,000
50,000	5.0	0	0	0-360	0	365	5 Gyrs	5.0×10^{-1}	1,000
60,000	5.0	0	0	0-360	0	365	5 Gyrs	5.0×10^{-1}	1,000
70,000	5.0	0	0	0-360	0	365	5 Gyrs	3.0×10^{-1}	1,000
80,000	5.0	0	0	0-360	0	365	5 Gyrs	1.0×10^{-1}	1,000

【Initial conditions of "80% tidal force model comet set"】 $(\overrightarrow{f_{tide80\%}} = -0.8 \times 4\pi G\rho\overrightarrow{z'})$

a_i [au]	q_i [au]	I_i [deg.]	Ω_i [deg.]	ω_i [deg.]	t [day]	tp [day]	Calculation time	ϵ	Number
20,000	5.0	0	0	0-360	0	365	5 Gyrs	8.0×10^{-1}	100
30,000	5.0	0	0	0-360	0	365	5 Gyrs	8.0×10^{-1}	100
40,000	5.0	0	0	0-360	0	365	5 Gyrs	5.0×10^{-1}	100
50,000	5.0	0	0	0-360	0	365	5 Gyrs	5.0×10^{-1}	100
60,000	5.0	0	0	0-360	0	365	5 Gyrs	5.0×10^{-1}	100
70,000	5.0	0	0	0-360	0	365	5 Gyrs	3.0×10^{-1}	100
80,000	5.0	0	0	0-360	0	365	5 Gyrs	1.0×10^{-1}	100

【Initial conditions of "120% tidal force model comet set"】

$(\overrightarrow{f_{tide120\%}} = -1.2 \times 4\pi G\rho\overrightarrow{z'})$

a_i [au]	q_i [au]	I_i [deg.]	Ω_i [deg.]	ω_i [deg.]	t [day]	tp [day]	Calculation time	ϵ	Number
20,000	5.0	0	0	0-360	0	365	5 Gyrs	8.0×10^{-1}	100
30,000	5.0	0	0	0-360	0	365	5 Gyrs	8.0×10^{-1}	100
40,000	5.0	0	0	0-360	0	365	5 Gyrs	5.0×10^{-1}	100
50,000	5.0	0	0	0-360	0	365	5 Gyrs	5.0×10^{-1}	100
60,000	5.0	0	0	0-360	0	365	5 Gyrs	5.0×10^{-1}	100
70,000	5.0	0	0	0-360	0	365	5 Gyrs	3.0×10^{-1}	100
80,000	5.0	0	0	0-360	0	365	5 Gyrs	1.0×10^{-1}	100

Appendix B − Relationship between the initial semi-major axis and comets' approach

In Section 3.2, we analyzed the relationship between the original semi-major axis (a_0) and the comets' approach. In this section, we focus on the "initial" semi-major axis (a_i) in order to reveal the dependency on the initial conditions. We must note that the initial semi-major axis is extremely difficult to be derived by the orbital calculation, so it is not realistic to use this parameter as the DNC criterion.

Fig. 47 shows the ratio of the number of comets that have approached closer than the snow line more than once for each initial semi-major axis. The fractions in the following graph show the ratio of the comets which have approaching history. The denominators indicate the number of model comets that have each initial semi-major axis as the initial condition, and the numerators indicate the number of comets that have an approaching history. The sum of the denominators ($n = 5{,}353$) does not equal the total number of model comets ($N_{all} = 7{,}000$). This is because some model comets change their orbits to hyperbola orbits during their journey due to the effect of external forces, and they are excluded. Fig. 48 shows the converted result of Fig. 47 into the DNC ratio by subtracting the percentage of each band from 100.

As a result, the global tendency is similar to that of the case of the original semi-major axis. However, the possibility of comets being DNCs gets to be 100% at $a_i \geq 70{,}000$ au. Therefore, it is obvious that the approaching history of comets has something to do with the initial condition. This shows the possibility that human beings might be able to reveal the initial state of the Solar system by investigating the current orbit of comets. More studies on the relationship between the initial conditions and the current orbit of comets must be conducted.

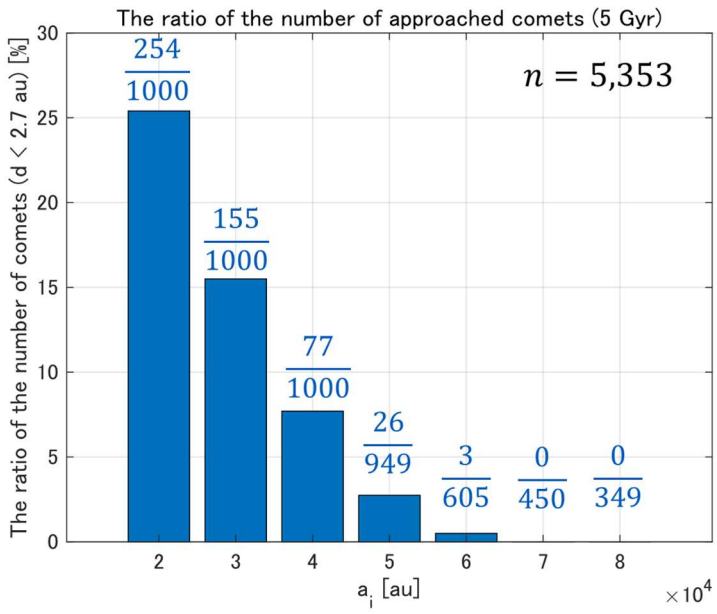

Fig. 47 The ratio of the number of comets which have approached closer than the snow line more than once for each initial semi-major axis (5 Gyrs).

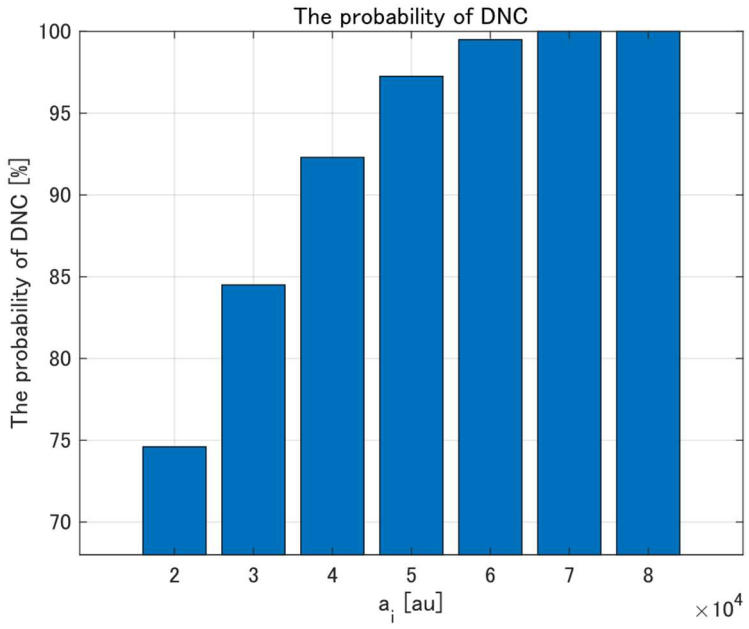

Fig. 48 The probability of comets being DNCs for each a_i.

References

A'Hearn, M. F., Millis, R. C., Schleicher, D. G., Osip, D. J., & Birch, P. V. (1995). The Ensemble Properties of Comets: Results from Narrowband Photometry of 85 Comets, 1976-1992. *Icarus, 118*(2), 223-270.

Astronomical Society of Japan. (2023, 01 10). *Astro-dictionary*. Retrieved from Oort Cloud: https://astro-dic.jp/

Batygin, K., & Laughlin, G. (2015). Jupiter's decisive role in the inner Solar System's early evolution. *Proceedings of the National Academy of Sciences of the United States of America, 112*(14), 4214-4217.

Binney, J., & Tremaine, S. (2008). *Galactic Dynamics.* Princeton University Press.

Bottke, W. F., Durda, D. D., Nesvorný, D., Jedicke, R., Morbidelli, A., Vokrouhlický, D., & Levison, H. F. (2005). Linking the collisional history of the main asteroid belt to its dynamical excitation and depletion. *Icarus, 179*(1), 63-94.

Dones, L., Weissman, P. R., Levison, H. F., & Duncan, M. J. (2004). Oort Cloud Formation and Dynamics. University of Arizona Press.

Duncan, M., Quinn, T., & Tremaine, S. (1987). The formation and extent of the solar system comet cloud. *The Astronomical journal, 94*(5), 1330.

Dybczyński,, P. (2023, 02 28). Retrieved from StePPeD - the Stellar Potential Perturbers Database, v. 3.1: https://pad2.astro.amu.edu.pl/StePPeD/index.php?n=Stars30.Downloads1

Eugene, M. F., & Wiliam, W. J. (2008). *Solar System Astrophysics.* Springer New York.

Festou, M., Keller, H., & Weaver, H. (2004). *Comets II.* University of Arizona Press.

Hairer, E., Nørsett, S. P., & Wanner, G. (1993). *Solving Ordinary Differential Equations I Nonstiff Problems.* Springer Berlin Heidelberg.

Heisler, J., & Tremaine, S. (1986). The influence of the Galactic tidal field on the Oort comet cloud. *Icarus, 65*(1), 12-26.

Higuchi, A. (2020). Anisotropy of Long-period Comets Explained by Their Formation Process. *The Astronomical Journal, 160*(3), 134.

Higuchi, A., & Kokubo, E. (2015). EFFECT of STELLAR ENCOUNTERS on COMET CLOUD FORMATION. *Astronomical Journal, 150*(1), 26.

Higuchi, A., Kokubo, E., Kinoshita, A., & Mukai, T. (2007). Orbital Evolution of Planetesimals due to the Galactic Tide: Formation of the Comet Cloud. *The Astronomical Journal, 134*(4), 1693-1706.

Holmberg, J., & Flynn, C. (2004). The local surface density of disc matter mapped by Hipparcos. *Monthly Notices of the Royal Astronomical Society, 352*(2), 440-446.

Jet Propulsion Laboratory (JPL), California Institute of Technology, NASA. (2023, 02 28). *Small-Body Database Lookup*. Retrieved from Solar System Dynamics: https://ssd.jpl.nasa.gov/tools/sbdb_lookup.html#/

Kinoshita, H., & Nakai, H. (2007). General solution of the Kozai mechanism. *Celestial Mechanics and Dynamical Astronomy, 98*(1), 67-74.

Kozai, Y. (1962). Secular Perturbations of Asteroids with High Inclination and Eccentricity. *The Astronomical Journal, 67*(1997), 579.

Królikowska, M., & Dybczynski, P. A. (2017). Oort spike comets with large perihelion distances. *Monthly Notices of the Royal Astronomical Society, 472*(4), 4634-4658.

Marsden, B. G., Sekanina, Z., & Yeomans, D. (1973). Comets and nongravitational forces. V. *The Astronomical Journal, 78*(2), 211-225.

Miida, Y., & Suda, H. (2014). *Suuchi-keisanho (Methods of numerical calculation) 2nd edition* . Morikita Publishing Co., Ltd.

Mondal, S., Roy, S., & Das, B. (2016). Numerical Solution of First-Order Linear Differential Equations in Fuzzy Environment by Runge-Kutta-Fehlberg Method and Its Application. *International Journal of Differential Equations, 2016*(2).

NASA, ESA, & Jian-Yang, L. (2023, 2 28). *Comet 252P/LINEAR*. Retrieved from ESA/Hubble: https://esahubble.org/images/opo1614b/

Oort, J. (1950). *The structure of the cloud of comets surrounding the Solar System and a hypothesis concerning its origin.* BAN.

The Astronomical Almanac. (2021). Astronomical Constants. *The Astronomical Almanac Online!*

Vokrouhlický, D., Nesvorný, D., & Dones, L. (2019). *Origin and Evolution of Long-period Comets.* The Astronomical Journal.

Weissman, P. R. (1990). The Oort Cloud. *Nature, 344*(6269), 825-830.

Yoshida, H. (1994). Kahen-jikan suteppu ni yoru shimpurekutikku suuchi kaiho (Hisenkei kahensekibunkei ni yoru ouyou kaiseki), (The symplectic integrator in variable steps; Applied analysis with non-linear inregrable systems). *Research Institute for Mechanical Sciences (RIMS) Kokyuroku, 889*, 70-76.

Acknowledgments

I would like to express my deep gratitude to my supervisor, Lecturer Kazuo Yoshioka. His kind instructions enabled me to accomplish this work. The fruitful discussions with him were so stimulating.

I am sincerely grateful to Professor Ichiro Yoshikawa, Professor Tsuyoshi Imamura and Lecturer Shohei Aoki. They gave me a lot of precious advice in the seminars.

I also gratefully thank the members of our laboratory, Mr. Yudai Suzuki, Mr. Hiromasa Akadama, Mr. Tatsuki Kosugi, Mr. Ashita Yamazaki, Mr. Kazushi Goda, Mr. Tatsuki Matsumoto and Ms. Saniya Sanada. Their valuable advice and opinions helped this work to make progress.

Finally, I would like to express my deepest thank to my family members including my parents, grandparents and my sister, who have supported my learning. This work could not have been accomplished without their kind support.